

Constraining A_4 Leptonic Flavour Model Parameters at Colliders and Beyond

Lukas Heinrich,^a Holger Schulz,^b Jessica Turner^c and Ye-Ling Zhou^d

^a*Physics Department, New York University, New York, NY 10003, U.S.A.*

^b*Department of Physics, University of Cincinnati, Cincinnati, OH 45219, U.S.A.*

^c*Theoretical Physics Department, Fermi National Accelerator Laboratory, P.O. Box 500, Batavia, IL 60510, U.S.A.*

^d*School of Physics and Astronomy, University of Southampton, Southampton, SO17 1BJ, U.K.*

E-mail: lh1132@nyu.edu, schulzhg@ucmail.uc.edu, jturner@fnal.gov,
ye-ling.zhou@soton.ac.uk

ABSTRACT: The observed pattern of mixing in the neutrino sector may be explained by the presence of a non-Abelian, discrete flavour symmetry broken into residual subgroups at low energies. Many flavour models require the presence of Standard Model singlet scalars which can promptly decay to charged leptons in a flavour-violating manner. We constrain the model parameters of a generic A_4 leptonic flavour model using a synergy of experimental data including limits from charged lepton flavour conversion, an 8 TeV collider analysis and constraints from the anomalous magnetic moment of the muon. The most powerful constraints derive from the MEG collaborations' limit on $\text{Br}(\mu \rightarrow e\gamma)$ and the reinterpretation of an 8 TeV ATLAS search for anomalous productions of multi-leptonic final states. We quantify the exclusionary power of each of these experiments and identify regions where the constraints from collider and MEG experimental data are complementary.

Contents

1	Introduction	1
2	The A_4 Leptonic Flavour Model	3
2.1	Basic Mechanism	3
2.2	A_4 Leptonic Flavour Models	4
2.3	Interactions Relevant for Phenomenology	6
3	Confronting the Model with Experimental Data	11
3.1	$g - 2$	12
3.2	MEG Result on $\text{Br}(\mu \rightarrow e\gamma)$	13
3.3	Higgs-Scalar Mixing Constraint	14
3.4	Higgs-Width Constraint	15
3.5	Reinterpretation of ATLAS Search for High Multiplicity Leptonic Final States	15
3.5.1	General Workflow	15
3.5.2	The ATLAS Search Analysis	16
3.5.3	Event Simulation and Analysis	19
3.5.4	The CLs Method	20
4	Results	21
5	Summary	28
A	Group Theory for A_4	31
B	Higgs Width Constraint	31

1 Introduction

Since the discovery of neutrino oscillations by Super-Kamiokande [1], two puzzling aspects of neutrino physics have emerged. First, neutrinos have very small but non-zero masses and second, the leptonic mixing or Pontecorvo-Maki-Nakagawa-Sakata (PMNS) matrix, U , has a strikingly different structure from the quark mixing matrix. One of the most fruitful beyond the Standard Model (SM) ideas applied to the neutrino sector is the introduction of a non-Abelian flavour symmetry to explain the observed structure of the PMNS matrix. These models generally propose a discrete flavour symmetry which is broken spontaneously, leaving the leptonic mass terms invariant under residual symmetries. Through symmetry considerations alone, without the specification of a detailed flavour model, it is possible to reduce the number of degrees of freedom between mixing parameters and thereby predict

sum-rules which will be testable at upcoming long (T2HK and DUNE) [2, 3] and medium (JUNO) [4] baseline neutrino oscillation experiments.

The popularity of the flavour symmetry paradigm is reflected in the sheer number of flavour symmetry groups that have been considered: from continuous ones such as $U(1)$ [5], $SO(3)$ [6, 7], $SU(3)$ [8, 9], and also the discrete cases Z_n [10, 11], A_4 [12–14], A_5 [15–17], S_4 [18, 19], $\Delta(27)$ [20, 21], $\Delta(48)$ [22, 23], etc. For a comprehensive review see e.g., Refs [24–26]. In a model-independent manner various leading order mixing patterns emerge as a result of flavour symmetries and their possible breaking such as tribimaximal (TBM) [27–30], golden-ratio (GR) [31–34] and bimaximal (BM) mixing [35–39]. In order to render the structure of the leptonic mixing compatible with data, in particular with the observation of a non-zero reactor mixing angle $\theta_{13} \approx 8^\circ$ [40–43], corrections to these mixing patterns are necessary.

Such a task can be completed in a model-independent or dependent manner. In the latter case, the breaking of the flavour symmetry is realised by SM singlet scalar fields, also known as *flavons*, which have non-trivial quantum numbers associated to the non-Abelian flavour group. These flavons acquire vacuum expectation values (VEVs) which spontaneously break the flavour symmetry to its Abelian residual symmetries in the charged lepton and neutrino sector. In general, two flavons are sufficient; however for larger symmetry groups and supersymmetric setups additional flavon multiplets are necessary for model construction [22, 23, 32, 33, 39, 44–53]. Typically, the corrections to the leading order mixing pattern are provided by higher dimensional operators formed between the flavons and charged leptons [24–26]. An alternative possibility was proposed in the work of [54], where the cross-coupling between the flavons of the neutrino and charged lepton sector may slightly break the Abelian residual symmetries and thereby provide the needed deviation from exact TBM mixing in the context of an A_4 flavour model.

The rich phenomenology of flavour models has been explored in the quark and lepton sector using both Abelian and non-Abelian flavour symmetries. In the case of Abelian family symmetries, which manifests from the Froggatt-Nielsen (FN) mechanism [5], the collider and flavour violating phenomenology of a single flavon was explored [55]. Although our model and theirs markedly differ, we reach a similar conclusion to their work: limits from MEG can largely exclude the flavour breaking scale of less than ~ 1 TeV. In addition, there has been work completed on constraining quark flavour model parameter space using collider constraints including Higgs-flavon mixing, electroweak oblique parameters and direct production of the flavon at current and future colliders [56–58]. Moreover, the observed flavour violating decay of the Higgs ($h \rightarrow \mu\tau$) was investigated in the context of a FN mechanism [59].

Using non-Abelian discrete symmetries the CLFV processes in A_4 was first discussed in [60], where channels allowed by the residual symmetry \mathbb{Z}_3 were emphasised. CLFV processes mediated by flavons were studied in [61, 62]. Specifically, correlations between \mathbb{Z}_3 -breaking channels and the correction to TBM were discovered in [62]. Constraints on the flavon mass in supersymmetric A_4 leptonic flavour models have been studied [63]. Moreover, the observed flavour violating decay of the Higgs ($h \rightarrow \mu\tau$) was investigated in the context of A_4 [64]. It was found that the flavon could be produced at colliders if it is sufficiently light.

There is also prospect for direct production, without reliance upon the flavon-Higgs mixing, at lepton colliders [65].

The primary aim of this work is to exclude regions of parameter space of a non-supersymmetric A_4 leptonic flavour model. To do so we apply a synergy of experimental data ranging from the reinterpretation an 8 TeV collider analysis to applying limits from charged lepton flavour violating (CLFV) processes determined by the MEG collaboration. To our best knowledge we are the first to undertake such a rigorous investigation of a relatively generic leptonic flavour model [62]. We begin with a discussion of the motivation for and the basic principles underlying leptonic flavour models. We further elucidate on the specific model in Section 2.2 with a particular emphasis on the relevant interactions for the 8 TeV ATLAS analysis and charged lepton flavour violation limits we recast. In Section 3 we discuss the model parameter space and sampling strategy. We first confront the model with experimental data from $g - 2$ and MEG as detailed in Section 3.1 and Section 3.2 respectively. The implementation of the Higgs-scalar mixing and Higgs width constraints are presented in Section 3.3 and Section 3.4 respectively. The aforementioned constraints can be calculated analytically; however, excluding regions of the parameter space using a collider data reinterpretation is a more involved process and the tool-chain, ATLAS analysis and CLs method are discussed at length in Section 3.5. Finally, we present our results and make concluding remarks in Section 4 and Section 5.

2 The A_4 Leptonic Flavour Model

2.1 Basic Mechanism

The threefold repetition of fermion generations and their subsequent masses and mixing structure, is arguably one of the most puzzling features of the SM. One plausible explanation of the pattern of fermionic mixing is an underlying flavour symmetry. In regards to the lepton sector, non-Abelian, discrete groups are a popular choice of family symmetry. This derives from the observation that leptonic mixing is large and generically, before the reactor mixing angle was measured, the entries of the PMNS matrix resembled Clebsch-Gordan coefficients of discrete groups.

The basic premise of leptonic flavour models is that at sufficiently high-energies there exists an underlying family symmetry, typically non-Abelian and discrete, which unifies the three generations of leptonic doublets into a single mathematical structure, such as a triplet of the flavour group. From the observation of neutrino oscillations, it is clear that leptonic masses are non-degenerate and therefore the non-Abelian flavour group cannot be a symmetry of the low-energy effective Lagrangian. As a consequence, it is assumed that the full flavour symmetry must be broken at low energies into two Abelian residual symmetry groups which are unbroken in the charged-lepton and neutrino sectors. The realisation of this breaking manifests through the introduction of new scalars, known as *flavons* which are usually assumed to be SM gauge singlets. The scalar potential of these flavons is invariant under transformations of the non-Abelian flavour symmetry at high-energies. However, at the *flavour breaking scale*, the non-trivial alignment of the VEVs of the flavons spontaneously break the non-Abelian flavour symmetry to Abelian residual

symmetries in the neutrino and charged lepton sectors. The forms of the residual symmetries derive from consideration of the largest possible symmetry of each sector and the structure inherited from the larger non-Abelian flavour group. The most general discrete residual symmetry of the charged lepton sector is a direct product of cyclic groups, \mathbb{Z}_n . In contrast, the largest symmetry of the complex, symmetric Majorana neutrino mass matrix is $\mathbb{Z}_2 \times \mathbb{Z}_2$. However, it is possible a subgroup thereof, namely \mathbb{Z}_2 , could be a residual symmetry of the neutrino mass matrix. These remnant symmetries constrain the structure of the charged lepton and neutrino mass matrices and thereby the structure of the leptonic mixing matrix.

2.2 A_4 Leptonic Flavour Models

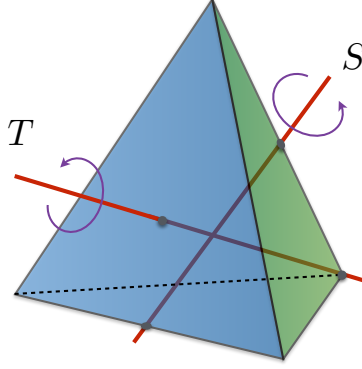


Figure 1: The tetrahedral group A_4 as the full flavour symmetry and its subgroups $T = \mathbb{Z}_3$ and $S = \mathbb{Z}_2$ as residual symmetries in the charged lepton and neutrino sectors, respectively.

In this work, we begin with the general A_4 model setup. The tetrahedral group or the rotational symmetries of a tetrahedron (A_4), as geometrically represented in Fig. 1, is the smallest discrete group (order 12) containing three-dimensional irreducible representations. The generators of the group, T and S , satisfy the relations: $T^3 = S^2 = (ST)^3 = \mathbb{1}$. This group contains four irreducible representations: three singlets $\mathbf{1}$, $\mathbf{1}'$, $\mathbf{1}''$, and one triplet, $\mathbf{3}$. In the Altarelli-Feruglio basis, the triplet representation matrices of generators S and T are given by

$$T = \begin{pmatrix} 1 & 0 & 0 \\ 0 & \omega^2 & 0 \\ 0 & 0 & \omega \end{pmatrix}, \quad S = \frac{1}{3} \begin{pmatrix} -1 & 2 & 2 \\ 2 & -1 & 2 \\ 2 & 2 & -1 \end{pmatrix}, \quad (2.1)$$

where $\omega = e^{2i\pi/3}$. T and S are respectively the generator of the residual symmetries $\mathbb{Z}_3 = \{\mathbb{1}, T, T^2\}$ and $\mathbb{Z}_2 = \{\mathbb{1}, S\}$ after A_4 symmetry breaking. The only physically inequivalent Abelian subgroups of A_4 are \mathbb{Z}_3 and \mathbb{Z}_2 where all other Abelian subgroups are conjugate to either \mathbb{Z}_3 or \mathbb{Z}_2 .

In flavour model building, at least two triplet flavons are required: one is needed for charged lepton and the other for neutrino mass generation. We denote these flavons as φ and χ , respectively. These flavons could be a pseudo-real or a complex triplet of A_4 . In this present work, we focus on the former scenario where the three components of φ

satisfy $\varphi_1 = \varphi_1^*$ and $\varphi_2 = \varphi_3^*$. Such an assumption allows for the minimal number of model parameters and degrees of freedom.

In most A_4 models, the electroweak leptonic doublets (denoted as $L = (L_e, L_\mu, L_\tau)^T$ with $L_e = (\nu_{eL}, e_L)^T$, $L_\mu = (\nu_{\mu L}, \mu_L)^T$ and $L_\tau = (\nu_{\tau L}, \tau_L)^T$) are often arranged to belong to a $\mathbf{3}$ of A_4 . And the right-handed charged leptons e_R , μ_R and τ_R belong to singlets $\mathbf{1}$, $\mathbf{1}'$ and $\mathbf{1}''$, respectively. The Higgs, H , is assigned as a trivial singlet $\mathbf{1}$ of A_4 . At leading order, the general Lagrangian terms responsible for lepton masses have the following form

$$\begin{aligned} -\mathcal{L}_l &= \frac{y_e}{\Lambda} (\bar{L}\varphi)_1 e_R H + \frac{y_\mu}{\Lambda} (\bar{L}\varphi)_{1''} \mu_R H + \frac{y_\tau}{\Lambda} (\bar{L}\varphi)_{1'} \tau_R H + \text{h.c.}, \\ -\mathcal{L}_\nu &= \frac{y_1}{2\Lambda\Lambda_W} ((\bar{L}\tilde{H}\tilde{H}^T L^c)_3 \chi)_1 + \frac{y_2}{2\Lambda_W} (\bar{L}\tilde{H}\tilde{H}^T L^c)_1 + \text{h.c.}, \end{aligned} \quad (2.2)$$

where $\tilde{H} = i\sigma_2 H^*$ and the subscript \mathbf{r} ($\mathbf{r} = \mathbf{1}, \mathbf{1}', \mathbf{1}'', \mathbf{3}$) denotes the irreducible¹ \mathbf{r} -plet product of the fields in the bracket. The scale Λ is a new scale higher than v_φ, v_χ and may arise as a consequence of the decoupling of some heavy A_4 multiplet particles. In order to generate tiny Majorana neutrino masses, we apply the traditional dimension-five Weinberg operator $(\bar{L}\tilde{H}\tilde{H}^T L^c)$ where Λ_W is the related scale, which may be different from Λ ².

The most widely studied mixing pattern is TBM mixing which predicts $\sin\theta_{12} = 1/\sqrt{3}$, $\sin\theta_{23} = 1/\sqrt{2}$ and $\sin\theta_{13} = 0$. Naturally, corrections are required to render TBM mixing consistent with neutrino oscillation data, in particular with the non-zero valued reactor angle, $\theta_{13} \approx 8^\circ$. One great success of A_4 models is that they naturally predict TBM mixing (at leading order) based on the following symmetry argument.

In order to ensure \mathbb{Z}_3 and \mathbb{Z}_2 as residual symmetries in charged lepton and neutrino sectors respectively, the vacuum alignment of these flavons is preserved under transformation of the residual symmetries

$$T\langle\varphi\rangle = \langle\varphi\rangle, \quad S\langle\chi\rangle = \langle\chi\rangle. \quad (2.3)$$

As a consequence, VEVs of φ and χ have to take the following forms

$$\langle\varphi\rangle = \begin{pmatrix} 1 \\ 0 \\ 0 \end{pmatrix} v_\varphi, \quad \langle\chi\rangle = \begin{pmatrix} 1 \\ 1 \\ 1 \end{pmatrix} \frac{v_\chi}{\sqrt{3}}, \quad (2.4)$$

respectively. Substituting these VEVs into Eq. (2.2), in addition to the electroweak symmetry breaking VEV of the Higgs $\langle H \rangle = v_H/\sqrt{2}$ with $v_H = 246$ GeV, we obtain the lepton mass matrices

$$m_l = \begin{pmatrix} y_e & 0 & 0 \\ 0 & y_\mu & 0 \\ 0 & 0 & y_\tau \end{pmatrix} \frac{v_H v_\varphi}{\sqrt{2n\Lambda}}, \quad m_\nu = \begin{pmatrix} 2a+b & -a & -a \\ -a & 2a & -a+b \\ -a & -a+b & 2a \end{pmatrix}, \quad (2.5)$$

¹We note that a brief recap on the representation theory of A_4 can be found in Appendix A.

² \mathcal{L}_ν in Eq. (2.2) differs from that in [54] by the UV completion. In the latter case, the right-handed neutrino, as the UV completion, has been explicitly written out. The simplification in this paper does not influence the studies of flavon in the charged lepton sector.

where $a \equiv y_1 v_\chi v_H^2 / (4\sqrt{3}\Lambda\Lambda_W)$ and $b \equiv y_2 v_H^2 / (2\Lambda_W)$. We note that the mass matrices of the charged lepton (m_l) and neutrino (m_ν) satisfy the aforementioned residual symmetries in the following manner:

$$T m_l m_l^\dagger T^\dagger = m_l m_l^\dagger, \quad S m_\nu S^T = m_\nu, \quad (2.6)$$

in which T and S are the generators of \mathbb{Z}_3 and \mathbb{Z}_2 , respectively, as mentioned before.

In order to generate a leptonic mixing matrix consistent with current global fit data [66], there must be a slight breaking of either the residual symmetry of the neutrino or charged lepton sector or possibly both. Although radiative corrections from the SM break the exact TBM mixing, such contributions are too small to induce $|U_{e3}| \approx 0.1$. It is possible that the necessary deviations from TBM result from higher order operators in the flavon potential or couplings between flavon and charged lepton sector (for reviews see e.g. [24–26]). Such cross-couplings result in a VEV shift, i.e., $\langle \varphi_2 \rangle \neq 0$, which thereby breaks the residual \mathbb{Z}_3 symmetry. Without loss of generality, one can always perform the following parameterisations

$$\langle \varphi_1 \rangle = v_\varphi, \quad \frac{\langle \varphi_2 \rangle}{\langle \varphi_1 \rangle} = \epsilon_\varphi. \quad (2.7)$$

Using this parametrisation, the shifted VEV $\langle \varphi \rangle$ can be always represented as

$$\langle \varphi \rangle = \begin{pmatrix} 1 \\ \epsilon_\varphi \\ \epsilon_\varphi^* \end{pmatrix} v_\varphi, \quad (2.8)$$

where ϵ_φ is a complex parameter. One requirement in this bottom-up approach is that, to be consistent with oscillation data, the \mathbb{Z}_3 -breaking effect should be small. In particular, the shift $|\epsilon_\varphi| \ll 1$. This shift could be one of the main sources of the deviations. In fact, as stated in [54], if we assume all corrections to the mixing are obtained from the φ VEV shift, θ_{13} and δ are predicted to be $\sin \theta_{13} = \sqrt{2} \text{Im}(\epsilon_\varphi)$ and $\delta = 270^\circ - 2 \text{Arg}(\epsilon_\varphi)$ for $\text{Im}(\epsilon_\varphi) > 0$. Furthermore, to be consistent with all oscillation data, ϵ_φ has to satisfy $0.10 \lesssim |\epsilon_\varphi| \lesssim 0.17$ and $38^\circ < \text{Arg}(\epsilon_\varphi) < 142^\circ$. However, in this work, we do not limit our discussion to a specific model. Instead, we will vary ϵ_φ in a relatively wide range, $|\epsilon_\varphi| \in [10^{-3}, 1]$ and $\text{Arg}(\epsilon_\varphi) \in [0, 2\pi)$ as shown in Table 1. Such an approach allows us to be agnostic about the origin of the corrections to the mixing; the needed correction could derive from a number of sources including the shift in the VEV of χ or higher dimensional operators responsible for the lepton masses.

2.3 Interactions Relevant for Phenomenology

We study the observable phenomenology of this well motivated flavour model and therefore concentrate on the interactions of the flavon associated with the charged lepton sector (φ). For the flavon χ in the neutrino sector, it has lesser experimental visibility³, which is why we do not consider its particle excitation and fix its VEV. The φ flavon communicates with

³Including non-standard interaction may lead to measurable effects of χ in neutrino oscillation experiments [67], but these effects are still small.

the SM in two ways. The first is via modification of the leptonic mass terms. The second is through the portal coupling of the flavons with the Higgs. In order to illustrate the effective interactions involving flavons, we expand the flavons and Higgs about their VEVs:

$$\varphi_i = \langle \varphi_i \rangle + \tilde{\varphi}_i, \quad \text{Re}(H^0) = \frac{v_H + \tilde{h}}{\sqrt{2}}. \quad (2.9)$$

For the charged-lepton-portal interaction, we can straightforwardly write the couplings between flavons and charged leptons from the Lagrangian terms of Eq. (2.2) in the Altarelli-Feruglio basis

$$\begin{aligned} -\mathcal{L}_{\text{clfc}}^{\tilde{h}, \tilde{\varphi}_1} &= \frac{m_e}{v_H} \bar{e} e \tilde{h} + \frac{m_\mu}{v_H} \bar{\mu} \mu \tilde{h} + \frac{m_\tau}{v_H} \bar{\tau} \tau \tilde{h} + \frac{m_e}{v_\varphi} \bar{e} e \tilde{\varphi}_1 + \frac{m_\mu}{v_\varphi} \bar{\mu} \mu \tilde{\varphi}_1 + \frac{m_\tau}{v_\varphi} \bar{\tau} \tau \tilde{\varphi}_1 \\ &\quad + \frac{m_e}{v_H v_\varphi} \bar{e} e \tilde{\varphi}_1 \tilde{h} + \frac{m_\mu}{v_H v_\varphi} \bar{\mu} \mu \tilde{\varphi}_1 \tilde{h} + \frac{m_\tau}{v_H v_\varphi} \bar{\tau} \tau \tilde{\varphi}_1 \tilde{h}, \\ -\mathcal{L}_{\text{clfv}}^{\tilde{\varphi}_2} &= \frac{m_e}{v_\varphi} (\bar{\mu}_L e_R \tilde{\varphi}_2 + \bar{\tau}_L e_R \tilde{\varphi}_2^*) + \frac{m_e}{v_H v_\varphi} (\bar{\mu}_L e_R \tilde{\varphi}_2 + \bar{\tau}_L e_R \tilde{\varphi}_2^*) \tilde{h} \\ &\quad + \frac{m_\mu}{v_\varphi} (\bar{\tau}_L \mu_R \tilde{\varphi}_2 + \bar{e}_L \mu_R \tilde{\varphi}_2^*) + \frac{m_\mu}{v_H v_\varphi} (\bar{\tau}_L \mu_R \tilde{\varphi}_2 + \bar{e}_L \mu_R \tilde{\varphi}_2^*) \tilde{h} \\ &\quad + \frac{m_\tau}{v_\varphi} (\bar{e}_L \tau_R \tilde{\varphi}_2 + \bar{\mu}_L \tau_R \tilde{\varphi}_2^*) + \frac{m_\tau}{v_H v_\varphi} (\bar{e}_L \tau_R \tilde{\varphi}_2 + \bar{\mu}_L \tau_R \tilde{\varphi}_2^*) \tilde{h} + \text{h.c.} \end{aligned} \quad (2.10)$$

From Eq. (2.10), we observe that \tilde{h} and $\tilde{\varphi}_1$ partake in charged lepton flavour conserving (CLFC) interactions while $\tilde{\varphi}_2$ partakes in the CLFV interactions.

The Higgs-portal interaction is obtained from the scalar potential. In principle, the full scalar potential should include self-couplings of H , φ and χ , as well as their cross-couplings. However, as we ignore the excitation of χ , the scalar potential can be simplified and effectively represented as a potential involving only the self- and cross-couplings of H and φ , and the VEV of χ contributes as a correction to the potential.

The self-couplings of Higgs are identical to the SM Higgs potential, given by

$$V_{\text{self}}(H) = \mu_H^2 H^\dagger H + \lambda (H^\dagger H)^2, \quad (2.11)$$

where the minimum of this potential is achieved by $\mu_H^2 < 0$ and $\lambda > 0$. In the unitary gauge, the Higgs doublet takes the form, $\langle H \rangle = (0, v_H/\sqrt{2})^T$. The cross-coupling between χ and H , $H^\dagger H (\chi \chi)_1$, only corrects the quadratic coupling of the Higgs after χ acquires a VEV. Such a term can be absorbed by the redefinition of the parameter μ_H and need not be written out explicitly.

The flavon can communicate with the visible sector via the Higgs portal coupling which cannot be forbidden by imposing any symmetries. The only renormalisable A_4 -invariant operator is $(H^\dagger H)(\varphi \varphi)_1$. This part of the potential is given by

$$V_{\text{cross}}(H, \varphi) = \frac{1}{2} \epsilon H^\dagger H (\varphi_1^2 + 2|\varphi_2|^2), \quad (2.12)$$

where ϵ is a real parameter. As the Higgs is A_4 -invariant, the cross-coupling does not alter the φ VEV direction. Consequently, this cross-coupling term does not contribute to leptonic flavour mixing. As we shall see later, this term will lead to mixing between the Higgs and

flavon and therefore plays an important role for the flavon production at the Large Hadron Collider (LHC).

The self-couplings of φ is the origin of the breaking of A_4 to \mathbb{Z}_3 . To simplify the couplings, an additional Z'_2 symmetry (or a larger Abelian symmetry including the transformation $\varphi \rightarrow -\varphi$) is usually imposed. With these considerations in mind, the most general A_4 - and Z'_2 -invariant self-couplings of φ is given by

$$V_{\text{self}}(\varphi) = \frac{1}{2}\mu_\varphi^2 I_{1\varphi} + \frac{g_1}{4} I_{1\varphi}^2 + \frac{g_2}{4} I_{2\varphi}, \quad (2.13)$$

where

$$I_{1\varphi} = \varphi_1^2 + 2|\varphi_2|^2, \quad I_{2\varphi} = \frac{1}{3}\varphi_1^4 - \frac{2}{3}\varphi_1(\varphi_2^3 + \varphi_2^{*3}) + |\varphi_2|^4. \quad (2.14)$$

In order to achieve a nontrivial and stable vacuum, the conditions $\mu_\varphi^2 < 0$ and $g_1 + g_2/3 > 0$ are required and applied throughout this work.

With the present terms of the Higgs and flavon potential (c.f. Eq. (2.11) and Eq. (2.13)), after spontaneous flavour breaking the leptonic mixing matrix would have exact TBM structure. In order to achieve the necessary deviation needed, the cross-coupling terms between charged lepton and neutrino flavons must be present. The cross-couplings between the Higgs and χ can be absorbed by the redefinition of μ_H^2 and therefore the only cross-coupling term left is the \mathbb{Z}_3 -breaking one, $(\varphi\varphi)_{\mathbf{1}''}(\chi\chi)_{\mathbf{1}'}$. This term is effectively represented as

$$V_{\mathbb{Z}_3}(\varphi) = \frac{1}{2}A(\varphi_2^2 + 2\varphi_1\varphi_2^*) + \text{h.c.}, \quad (2.15)$$

where A is a complex parameter with mass dimension two. The other cross-couplings are trivial. For example, $(\varphi\varphi)_{\mathbf{1}}(\chi\chi)_{\mathbf{1}}$ with $\chi = \langle\chi\rangle$ can be absorbed by the redefinition of μ_φ , and $(\varphi\varphi)_{\mathbf{3}}(\chi\chi)_{\mathbf{3}} = 0$ for the \mathbb{Z}_2 -preserving VEV $\langle\chi\rangle$.

Hence, the effective potential is constructed from Equations (2.11), (2.12), (2.13) and (2.15):

$$V(H, \varphi) = V_{\text{self}}(H) + V_{\text{cross}}(H, \varphi) + V_{\text{self}}(\varphi) + V_{\mathbb{Z}_3}(\varphi). \quad (2.16)$$

After minimisation of the Higgs and flavon potential, these parameters satisfy the following condition

$$\begin{aligned} \mu_H^2 + \lambda v_H^2 + \frac{1}{2}\epsilon v_\varphi^2(1 + 2|\epsilon_\varphi|^2) &= 0, \\ \mu_\varphi^2 + g_1 v_\varphi^2(1 + 2|\epsilon_\varphi|^2) + \frac{1}{3}g_2 v_\varphi^2[1 - \text{Re}(\epsilon_\varphi^3)] + \frac{1}{2}\epsilon v_H^2 + A\epsilon_\varphi^* + A^*\epsilon_\varphi &= 0, \\ \mu_\varphi^2 \epsilon_\varphi + g_1 v_\varphi^2(1 + 2|\epsilon_\varphi|^2)\epsilon_\varphi + \frac{1}{2}g_2 v_\varphi^2[-\epsilon_\varphi^{*2} + |\epsilon_\varphi|^2\epsilon_\varphi] + \frac{1}{2}\epsilon \epsilon_\varphi v_H^2 + A + A^*\epsilon_\varphi^* &= 0. \end{aligned} \quad (2.17)$$

We note that the shifted VEV, $\langle\varphi\rangle = (1, \epsilon_\varphi, \epsilon_\varphi^*)^T v_\varphi$, gives rise to non-zero θ_{13} and CP violation. The parameter A may be determined from Eq. (2.17) in the following manner

$$\begin{aligned} A\epsilon_\varphi^* + A^*\epsilon_\varphi^{*2} + 2\text{Re}(A^*\epsilon_\varphi)|\epsilon_\varphi|^2 &= \underbrace{-\frac{1}{2}g_2 v_\varphi^2 \epsilon_\varphi^{*3} + \frac{1}{3}g_2 v_\varphi^2 |\epsilon_\varphi|^2 \left[1 - \text{Re}(\epsilon_\varphi^3) - \frac{3}{2}|\epsilon_\varphi|^2\right]}_x \\ A &= \frac{(\epsilon_\varphi^*)^2 x^* - \epsilon_\varphi (x + 2i|\epsilon_\varphi|^2 \Im[x])}{|\epsilon_\varphi|^2 (-|\epsilon_\varphi|^2 + \epsilon_\varphi^{*3} + \epsilon_\varphi^3 - 1)}. \end{aligned} \quad (2.18)$$

We now consider the masses of the Higgs and flavons modified by the \mathbb{Z}_3 -breaking coupling. After the shifted VEV $\langle\varphi\rangle = (1, \epsilon_\varphi, \epsilon_\varphi^*)^T v_\varphi$ is included, the mixing between φ_1 and φ_2 , as well as the Higgs with φ_2 , is predicted. We obtain the mass term for all scalars in the basis $\tilde{\Phi} = (\tilde{h}, \tilde{\varphi}_1, \sqrt{2}\text{Re}(\tilde{\varphi}_2), \sqrt{2}\text{Im}(\tilde{\varphi}_2))^T$

$$-\mathcal{L}_{\text{scalar masses}} = \frac{1}{2}\tilde{\Phi}^\dagger M_\Phi^2 \tilde{\Phi}, \quad (2.19)$$

where the mass matrix M_Φ^2 is a real 4×4 symmetric matrix with the following entries

$$\begin{aligned} (M_\Phi^2)_{11} &= 2\lambda v_H^2, \\ (M_\Phi^2)_{22} &= 2(g_1 + \frac{g_2}{3})v_\varphi^2 + \frac{1}{3}g_2 v_\varphi^2 \text{Re}(\epsilon_\varphi^3) - 2\text{Re}(A\epsilon_\varphi^*), \\ (M_\Phi^2)_{33} &= -\frac{1}{3}g_2 v_\varphi^2 [1 - \text{Re}(\epsilon_\varphi^3)] + \frac{1}{2}g_2 v_\varphi^2 |\epsilon_\varphi|^2 - 2\text{Re}(A\epsilon_\varphi^*) + \text{Re}\left(-g_2 v_\varphi^2 (\epsilon_\varphi^* - \frac{1}{2}\epsilon_\varphi^2) + 2g_1 v_\varphi^2 \epsilon_\varphi^2 + A^*\right), \\ (M_\Phi^2)_{44} &= -\frac{1}{3}g_2 v_\varphi^2 [1 - \text{Re}(\epsilon_\varphi^3)] + \frac{1}{2}g_2 v_\varphi^2 |\epsilon_\varphi|^2 - 2\text{Re}(A\epsilon_\varphi^*) - \text{Re}\left(-g_2 v_\varphi^2 (\epsilon_\varphi^* - \frac{1}{2}\epsilon_\varphi^2) + 2g_1 v_\varphi^2 \epsilon_\varphi^2 + A^*\right), \\ (M_\Phi^2)_{12} &= v_H v_\varphi \epsilon, \\ (M_\Phi^2)_{13} &= \sqrt{2}v_H v_\varphi \epsilon \text{Re}(\epsilon_\varphi), \\ (M_\Phi^2)_{14} &= \sqrt{2}v_H v_\varphi \epsilon \text{Im}(\epsilon_\varphi), \\ (M_\Phi^2)_{23} &= \sqrt{2}\text{Re}\left(2g_1 v_\varphi^2 \epsilon_\varphi - \frac{1}{2}g_2 v_\varphi^2 \epsilon_\varphi^{*2} + A\right), \\ (M_\Phi^2)_{24} &= \sqrt{2}\text{Im}\left(2g_1 v_\varphi^2 \epsilon_\varphi - \frac{1}{2}g_2 v_\varphi^2 \epsilon_\varphi^{*2} + A\right), \\ (M_\Phi^2)_{34} &= \text{Im}\left(-g_2 v_\varphi^2 (\epsilon_\varphi^* - \frac{1}{2}\epsilon_\varphi^2) + 2g_1 v_\varphi^2 \epsilon_\varphi^2 + A^*\right), \end{aligned} \quad (2.20)$$

and $\tilde{\varphi}_1$ ($\tilde{\varphi}_2$) denotes the particle excitation around the VEV of φ_1 (φ_2), i.e., Eq. (2.9). Numerically, M_Φ^2 can be diagonalised by a real 4×4 orthogonal matrix W as $W^T M_\Phi^2 W = \text{diag}\{m_h^2, m_{s_1}^2, m_{s_2}^2, m_{s_3}^2\}$. The SM Higgs is denoted as h ($m_h = 125$ GeV)⁴ with the three other scalar mass eigenstates denoted as s_1, s_2, s_3 .

We relate the gauge to the mass basis in the following way:

$$\begin{pmatrix} \tilde{h} \\ \tilde{\varphi}_1 \\ \sqrt{2}\text{Re}(\tilde{\varphi}_2) \\ \sqrt{2}\text{Im}(\tilde{\varphi}_2) \end{pmatrix} = \begin{pmatrix} W_{00} & W_{01} & W_{02} & W_{03} \\ W_{10} & W_{11} & W_{12} & W_{13} \\ W_{20} & W_{21} & W_{22} & W_{23} \\ W_{30} & W_{31} & W_{32} & W_{33} \end{pmatrix} \begin{pmatrix} h \\ s_1 \\ s_2 \\ s_3 \end{pmatrix}. \quad (2.21)$$

Before we proceed we will summarise the model parameter space relevant for limit setting. From Eqs. (2.18) and (2.20), we observe this model contains the following parameters: $\epsilon, \epsilon_\varphi, v_\varphi, g_1, g_2$. We note that all the parameters are real apart from ϵ_φ and therefore there are six free parameters. Some salient features of this model include:

⁴Clearly, the SM quartic coupling is fixed once the mass matrix, M , is diagonalised and the $(1, 1)$ entry is fixed to be the Higgs mass squared.

- The parameter ϵ controls the cross-coupling of the flavons with SM Higgs. This parameter is of crucial importance for the Higgs-flavon mixing and therefore the production of flavons at colliders and will be further discussed in Section 3.5.
- ϵ_φ parametrises the breaking of \mathbb{Z}_3 in the charged lepton sector. As $\epsilon_\varphi \rightarrow 0$, the \mathbb{Z}_3 -preserving limit is reached and TBM mixing is recovered. Therefore, φ_2 does not acquire a VEV and the only mixing that occurs is between h and φ_1 . Subsequently, only CLFC interactions are present.
- The flavour breaking scale is parametrised by the VEV of φ : v_φ . Moreover, the masses of the flavons are functions of v_ϕ and therefore the presence of these flavons, at colliders or otherwise, will be increasingly suppressed as the flavour breaking scale becomes larger⁵.
- M^2 is diagonalised via $M^2 = W \hat{M}^2 W^T$, where \hat{M}^2 is a diagonal matrix and W is a real orthogonal matrix. In the case $|M_{ij}^2| \ll |M_{jj}^2 - M_{ii}^2|$, the non-diagonal entries of W are approximately given by

$$O_{ij} \approx \frac{M_{ij}^2}{M_{jj}^2 - M_{ii}^2}. \quad (2.22)$$

In the limit $M_{jj}^2 \approx M_{ii}^2$, the mixing between the scalars becomes ill defined. In order to avoid this regime, we explore regions of the parameter space where the flavon masses are non-degenerate⁶ and the three flavon masses lie outside a 10 GeV window of the Higgs mass as will be explained further in Section 3.5.

- In the majority of the parameter space the flavons can promptly decay to two charged leptons both in a manner which is charged lepton flavour conserving and violating. Moreover, as the coupling of the flavons to the charged leptons is proportional to the charged lepton mass, the dominant decay channel of the flavons is tau-dominated.
- g_1 and g_2 are dimensionless couplings present in the $A_4 \times Z'_2$ invariant flavon potential as shown in Eq. (2.13). Their role is most easily understood in the limit $\epsilon_\varphi \rightarrow 0$ where an exact \mathbb{Z}_3 residual symmetry in the charged lepton sector is recovered. In such a framework, φ_2 does not acquire a VEV, and masses of s_2 and s_3 are obtained from the quadratic terms of the scalar potential, $m_{s_2} = m_{s_3} = \sqrt{-\frac{1}{3}g_2 v_\varphi^2}$. However, φ_1 , does acquire a VEV and therefore mixes with the Higgs. Subsequently, the mass eigenstates of the Higgs and φ_1 are

$$m_h^2 = 2\lambda v_H^2 + \left(\lambda v_H^2 - \left(g_1 + \frac{g_2}{3} \right) v_\varphi^2 \right) \left(\sqrt{1 + \left(\frac{\epsilon v_H v_\varphi}{\lambda v_H^2 - \left(g_1 + \frac{g_2}{3} \right) v_\varphi^2} \right)^2} - 1 \right),$$

⁵Unfortunately for a 4×4 mass matrix there are no closed analytic form for the masses of s_1 , s_2 and s_3 ; however the masses are a complicated function of all the parameters in \mathbf{p} and are approximately linear in v_φ .

⁶We ensure the difference between the flavon masses is ≥ 10 MeV.

$$m_{s_1}^2 = 2(g_1 + \frac{g_2}{3})v_\varphi^2 + \left((g_1 + \frac{g_2}{3})v_\varphi^2 - \lambda v_H^2\right) \left(\sqrt{1 + \left(\frac{\epsilon v_H v_\varphi}{\lambda v_H^2 - (g_1 + \frac{g_2}{3})v_\varphi^2}\right)^2} - 1\right). \quad (2.23)$$

In the realistic regime we are interested in, namely $\epsilon_\varphi \neq 0$, the masses of m_{s_1} and m_{s_2} (m_{s_3}) are proportional to $(g_1 + g_2/3)$ and g_2 respectively⁷, however the relation no longer has a closed analytic as the 4×4 mass matrix must be diagonalised numerically.

3 Confronting the Model with Experimental Data

In the previous section, we reviewed the pertinent features of the model and presented its free parameters. The objective of this section is to evaluate the extent to which existing measurements are able to constrain the allowed parameter space. In order to do so, we compare predictions of the model with dedicated data from the $g - 2$, MEG and ATLAS experiments. The former two experimental limits can be directly compared with analytic calculations and are discussed in Section 3.1 and Section 3.2 respectively. The comparison of the model prediction with collider data requires a rather involved tool-chain based on Monte-Carlo event generators and analysis software. We discuss the signatures of this flavour model at the LHC, Monte-Carlo event generation, the ATLAS measurement and statistical methodology used in Section 3.5.

Parameter Space and Sampling

To simplify the numerical treatment, we apply the polar form of the complex parameter $\epsilon_\varphi = |\epsilon_\varphi| \cdot e^{i\theta_\varphi}$ and define our parameter space in terms of its magnitude and phase. In those cases where a model parameter spans several orders of magnitude, the sampling is performed logarithmically. The parameter sampling boundaries are given in Table 1.

Parameter \mathbf{p}	$\min(p)$	$\max(p)$
$\log_{10}(v_\varphi)$	1	3
$\log_{10}(\varepsilon)$	-3	0
$\log_{10}(g_1)$	-4	0
$\log_{10}(-g_2)$	-4	0
$\log_{10}(\epsilon_\varphi)$	-3	0
θ_φ	0	2π

Table 1: Parameter sampling boundaries.

Sampling Strategy

The sampling is undertaken in a random uniform fashion. By doing so, we ensure that samples from sub-spaces exhibit the same uniform structure as the global sampling space.

⁷We note in the Z_3 -preserving scenario $m_{s_2} = m_{s_3}$ but in the Z_3 -breaking case there is a splitting in those masses.

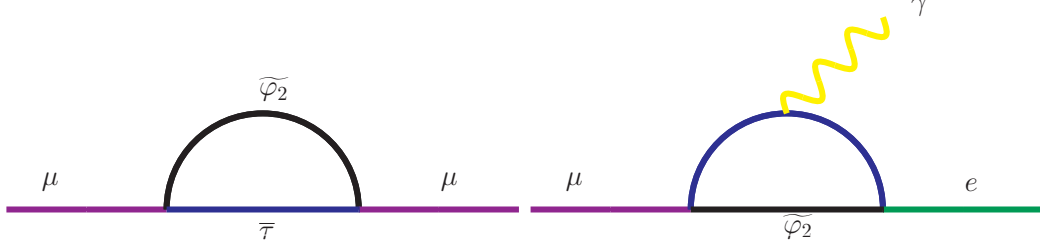


Figure 2: On the left is the leading one-loop contribution to the muon anomalous magnetic moment and on the right is the leading one-loop contribution to $\mu \rightarrow e\gamma$.

A sampled point is then used to construct the mass matrix, M_{Φ}^2 (Eq. (2.20)), which we diagonalise numerically. We *reject* a sampled point if any of the following conditions on the resulting scalar masses $m_{s_1}, m_{s_2}, m_{s_3}$ is fulfilled:

1. Any flavon mass is too light, i.e. $m_{s_i} < 10$ GeV, $i = 1, 2, 3$.
2. All flavon masses are > 1 TeV.
3. Any flavon mass is too close to the Higgs — $|m(s_i) - m_H| < 5$ GeV for $i = 1, 2, 3$.
4. Any flavon mass which is not the Higgs is close to being degenerate — $|m(s_i) - m(s_j)| < 100$ MeV for $i, j = 1, 2, 3$.
5. $\lambda(g_1 + \frac{g_2}{3}) < \frac{\varepsilon}{4}$.
6. $g_1 + \frac{g_2}{3} < 0$.

The conditions 1 and 2 ensure that the theory is well behaved and that the production cross-section of the new scalars is not too small while the requirements 3 and 4 protect against being in the regime of resonant mixing. The final two constraints 5, 6 guarantee vacuum stability [68] and that the scalar masses are positive.

All points sampled from the parameter space specified in Table 1 that pass all six prerequisites are further tested in terms of compatibility with experimental data as detailed in the following. The total number of points passing the aforementioned cuts is $N_{\text{tot}} = 8865$, which we found to be a sufficient number of points to cover the model parameter space. For each type of data, d , we count the number of points not excluded by it, $N_{\text{pass}}^{(d)}$, and calculate the exclusion power as $\frac{N_{\text{tot}} - N_{\text{pass}}^{(d)}}{N_{\text{tot}}}$. We summarise the exclusionary powers of the following experimental data in Section 4.

3.1 $g - 2$

The most recent measurements of the anomalous magnetic moment of the muon at Brookhaven National Laboratory (BNL) [69, 70] indicate a deviation from the Standard Model precision calculation. The Muon $g - 2$ experiment E989 based at Fermilab aims to make a factor of four improvement upon the current measurement [71].

New physics models, with additional scalars coupling to charged leptons, may explain this deviation. The muon anomalous magnetic moment is defined to be $a_\mu = (g - 2)_\mu / 2$ and its deviation from the SM is given by

$$\Delta a_\mu = a_\mu^{\text{exp}} - a_\mu^{\text{SM}} = (2.87 \pm 0.8) \times 10^{-9} \quad (3.6\sigma). \quad (3.1)$$

In the flavour model we investigate, the leading contribution to $g - 2$ has a τ -lepton running in the loop as shown in Fig. 2. Completing a standard calculation (see for example Refs. [72–74]) we find the magnetic moment to be

$$\Delta a_\mu = \frac{m_\mu^2 m_\tau^2}{24\pi^2 v_\varphi^2} \left[\frac{(|W_{20}|^2 - |W_{30}|^2)}{m_h^2} + \frac{(|W_{21}|^2 - |W_{31}|^2)}{m_{s_1}^2} + \frac{(|W_{22}|^2 - |W_{32}|^2)}{m_{s_2}^2} + \frac{(|W_{23}|^2 - |W_{33}|^2)}{m_{s_3}^2} \right]. \quad (3.2)$$

We note that there is a one-loop level contribution to Δa_μ from $\tilde{\varphi}_1$; however, as the couplings of each vertex $\propto m_\mu / v_\varphi$, there is a $\mathcal{O}(10^{-3})$ suppression relative to that of the process shown in Fig. 2 and therefore its contribution is negligible. In order to test whether a parameter point \mathbf{p} is excluded by the result in Eq. (3.1), we interpret the latter as an upper boundary on a_μ and demand that $\Delta a_\mu(\mathbf{p}) \leq 3.68 \times 10^{-9}$.

3.2 MEG Result on Br ($\mu \rightarrow e\gamma$)

SM processes which violate charged lepton flavour, induced by massive neutrinos, occur at unobservable rates $\sim \mathcal{O}(10^{-48})$. However, new physics models which modify the charged lepton sector could enhance such processes to detectable rates and provide crucial information in complement to direct searches. The \mathbb{Z}_3 -breaking flavour model discussed in Section 2.2 has both a rich flavour and chiral structure. Moreover, as the flavons couple to the charged leptons, such a model will alter CLFV rates.

There has been a systematic improvement in the sensitivity to a wide range of CLFV processes. The current bounds on the branching ratio of τ -CLFV radiative decays processes are $\sim \mathcal{O}(10^{-8})$ [75–77]. The upper limit on the branching ratio of $\mu \rightarrow e\gamma$ flavour conversion processes are currently $\sim \mathcal{O}(10^{-12})$ [77, 78] with the most stringent constraint from the MEG collaboration, with $\text{Br}(\mu \rightarrow e\gamma) \leq 4.2 \times 10^{-13}$ [79] at 90% C.L. A MEG upgrade (MEG II) is envisaged to further constrain the upper limit on this CLFV process to $\sim 4 \times 10^{-14}$ in the near term [80]. The Mu2e experiment at Fermilab [81] and COMET [82] based in JPARC aims to even further increase the sensitivity to this rare decay, $\leq 10^{-16} - 10^{-17}$.

Consequently, as the experimental constraint from $\mu \rightarrow e\gamma$ flavour conversion provides one of the most severe limits on CLFV processes, the implications of this limit in both supersymmetric and non-supersymmetric A_4 flavour models from higher dimensional operators has been studied in detail [83, 84].

For our scenario of \mathbb{Z}_3 -breaking scenario⁸ this process is loop-induced and is mediated by $\tilde{\varphi}_2$ as shown in Fig. 2. The contribution of the flavon in the loop was studied in great

⁸We note there are a number of other CLFV transitions which may occur in this model such as $\tau \rightarrow \mu\gamma$, $\tau \rightarrow e\gamma$, $\tau \rightarrow e\mu\mu$ and $\tau \rightarrow e\mu\mu$ [62]. However, as the limits placed on the branching ratio of these processes are relatively weak compared with the CLFV limit set by MEG, they will not offer stronger constraints.

detail in [62] where the assumption of small ϵ_φ was applied. In this present work, we do not apply this assumption.

The leading contribution to this CLFV process, as shown in Fig. 2, is mediated by φ_2 . Due to the flavour and chiral structure of the Yukawa couplings, the dominant contribution derives from φ_2 coupling to the τ charged leptons in the loop. This contribution towards $\text{Br}(\mu \rightarrow e\gamma)$ is calculated, in the mass basis, and is given below:

$$\text{Br}(\mu \rightarrow e\gamma) = \frac{\Gamma(\mu \rightarrow e\gamma)}{\Gamma(\mu \rightarrow e\bar{\nu}_e\nu_\mu)}, \quad (3.3)$$

where

$$\Gamma(\mu \rightarrow e\gamma) = \frac{m_\mu^3 |A|^2}{16\pi}, \quad \Gamma(\mu \rightarrow e\bar{\nu}_e\nu_\mu) = \frac{G_F^2 m_\mu^5}{192\pi^3}, \quad (3.4)$$

with

$$\begin{aligned} A(h) &= \frac{1}{128\pi^2} \frac{1}{m_h^2 v_\varphi^2} G_2 \left(\frac{m_\tau^2}{m_H^2} \right) \left[m_\mu m_\tau^2 (W_{20} + iW_{30})^2 - m_\mu m_\tau^2 \epsilon_\varphi^* (|W_{20}|^2 + |W_{30}|^2) \right], \\ A(s_1) &= \frac{1}{128\pi^2} \frac{1}{m_{s_1}^2 v_\varphi^2} G_2 \left(\frac{m_\tau^2}{m_H^2} \right) \left[m_\mu m_\tau^2 (W_{21} + iW_{31})^2 - m_\mu m_\tau^2 \epsilon_\varphi^* (|W_{21}|^2 + |W_{31}|^2) \right], \\ A(s_2) &= \frac{1}{128\pi^2} \frac{1}{m_{s_2}^2 v_\varphi^2} G_2 \left(\frac{m_\tau^2}{m_H^2} \right) \left[m_\mu m_\tau^2 (W_{22} + iW_{32})^2 - m_\mu m_\tau^2 \epsilon_\varphi^* (|W_{22}|^2 + |W_{32}|^2) \right], \\ A(s_3) &= \frac{1}{128\pi^2} \frac{1}{m_{s_3}^2 v_\varphi^2} G_2 \left(\frac{m_\tau^2}{m_H^2} \right) \left[m_\mu m_\tau^2 (W_{23} + iW_{33})^2 - m_\mu m_\tau^2 \epsilon_\varphi^* (|W_{23}|^2 + |W_{33}|^2) \right]. \end{aligned} \quad (3.5)$$

The functional form of G_2 is

$$G_2(x) = -\log x - \frac{11}{6}, \quad (3.6)$$

and finally A is given by the sum

$$A = A(h) + A(s_1) + A(s_2) + A(s_3). \quad (3.7)$$

Through the perturbative expansion of W_{ij} , using ϵ_φ as the expansion parameter, this result is consistent with that found in [62].

The calculation is straightforward and we can compare the flavon model prediction for $\text{Br}(\mu \rightarrow e\gamma)$ at any test point \mathbf{p} with the experimentally found upper limit. We expect and indeed find that MEG data provides the strongest exclusionary power of all the experiments as it is dedicated to search for flavour change. This is discussed in further detail in Section 4.

3.3 Higgs-Scalar Mixing Constraint

Extending the scalar sector of the SM has been a popular option to address various beyond SM phenomena such as providing a dark matter candidate [85–87]. Therefore, implications

on the Higgs sector in the context of a single pure scalar singlet have been explored in a number of works [88–92]. These works have constrained the mixing of the new scalar with the Higgs. In general, the mixing is small and the 125 GeV Higgs boson we observed at the LHC appears to be mostly comprised of the SM Higgs mass eigenstate. In our case, there are three additional scalars which acquire VEVs and therefore all three flavons mix with the Higgs. The constraint on \mathbf{p} enforced from mixing is imposed via the following requirement:

$$|W_{00}|^2 > 0.86.$$

3.4 Higgs-Width Constraint

In certain regions of the model parameter space, \mathbf{p} , it is possible that the coupling of s_1 , s_2 and s_3 to h will modify the Higgs total width. Theoretical calculations, assuming purely SM interactions, predict the Higgs total width (Γ_{SM}) to be ≈ 4 MeV. However, the constrained upper limits of the total width, using measurements of on- and off-shell decay rates to Z-bosons, indicate the upper limit to be 22 MeV at a 95% C.L. [93]. In such regions of the model parameter space, we assume that the deviation between the theoretically predicted and measured Higgs width derives entirely from new physics associated to our model as outlined in the Appendix⁹. We consider a point \mathbf{p} excluded by the Higgs-width results if the calculated width exceeds 22 MeV.

3.5 Reinterpretation of ATLAS Search for High Multiplicity Leptonic Final States

Reinterpreting a collider analysis is a more involved procedure compared to the experimental constraints discussed in the previous sections. We shall therefore initially give a brief explanation of the general workflow followed by more specific descriptions of the ATLAS analysis, event simulation and statistical methods applied.

3.5.1 General Workflow

We need to simulate fully differential collider events and analyse them as faithful to the original data analysis as possible in order to be able to compare predictions to the measured observation and background events. The procedure requires writing the physics model in question in a language a Monte-Carlo (MC) event generator is able to understand. We use FeynRules [94] to code the Lagrangian and derive a model file in the Universal FeynRules Output (UFO) format. This UFO format is understood by the MC event generator SHERPA [95, 96] which in turn is then able to simulate proton-proton collisions according to the flavon model including QCD and QED radiation effects as well as hadronisation and hadron decays.

The simulated events are analysed by the dedicated tool RIVET [97]. For the ATLAS analysis we have chosen to reinterpret, we are greatly helped by the fact that the analysis team provided a validated RIVET routine of their measurement. The latter contains exactly the same selection criteria and analysis logic as applied in the original data analysis. One

⁹In the new physics contributions to the Higgs width we ignore the three-body decays as these, in the majority of the phase space, are suppressed.

caveat, namely that the presented data and background distributions have not been corrected for detector effects (not “unfolded”) is overcome by the fact that the analysis team included a machinery that applies all resolutions and efficiencies to the simulated particles such that a fair comparison between our signal MC and the data is possible.

In order to make a statement on whether a sampled point \mathbf{p} yields a prediction that is compatible with the data we apply a hypothesis test known as the CL_s method. This method allows to distinguish, on a certain confidence level, whether the observed data is more likely to be explained by the SM background only or by the signal plus background hypothesis.

3.5.2 The ATLAS Search Analysis

There are many beyond SM (BSM) scenarios which have anomalous production of leptonic final states and therefore there have been a number of dedicated analyses which have searched for three or more charged, prompt and isolated leptons. These analyses have shown little deviation from the SM expectation and therefore may be effective in excluding regions of parameter space for many models. The ATLAS collaboration has conducted a number of supersymmetry searches which have multi-lepton final states [99–101] and indeed a model-independent analysis was performed, providing limits using 7 TeV data [102]. The CMS Collaboration has also performed a similar analysis using both 7 TeV [103] and 8 TeV data [104].

The analysis we choose to constrain our model parameter space, \mathbf{p} , uses a data sample collected in 2012 by the ATLAS experiment with a centre of mass energy of 8 TeV and corresponding integrated luminosity of 20.3 fb^{-1} [98]. This analysis searches for the anomalous production of at least three charged leptons in the final state. Moreover, as this analysis searches for events which have at least one tau final state, it is particularly well suited to our model as the flavons dominantly decay to taus and muons. The analysis logic and data have been preserved, validated and made publicly available by the ATLAS collaboration within the analysis tool RIVET [97] as **ATLAS_2014_I1327229**. We found this measurement, of all publicly available and validated analysis, to be the most suitable for constraining our model parameter space. We re-use the observed data and total background estimates published by ATLAS as presented in Table 4 to perform our statistical analysis.

We shall not reiterate the full details of the analysis but rather present the most relevant features for our work. The analysis first applies a veto on Z-bosons and then divides the events (which contain at least three leptons) into four disjoint signal regions based on charged lepton flavour pairs and leptonic content.

- **OSSF**: events which contain an opposite sign same flavour (OSSF) charged lepton pair.
- **no OSSF**: events which do not contain an OSSF pair.
- $\geq 3e/\mu$: events which contain minimally three electrons or muons.
- $2e/\mu \geq 1\tau_{\text{had}}$: events containing two electrons or muons with and at least one hadronically decaying tau lepton.

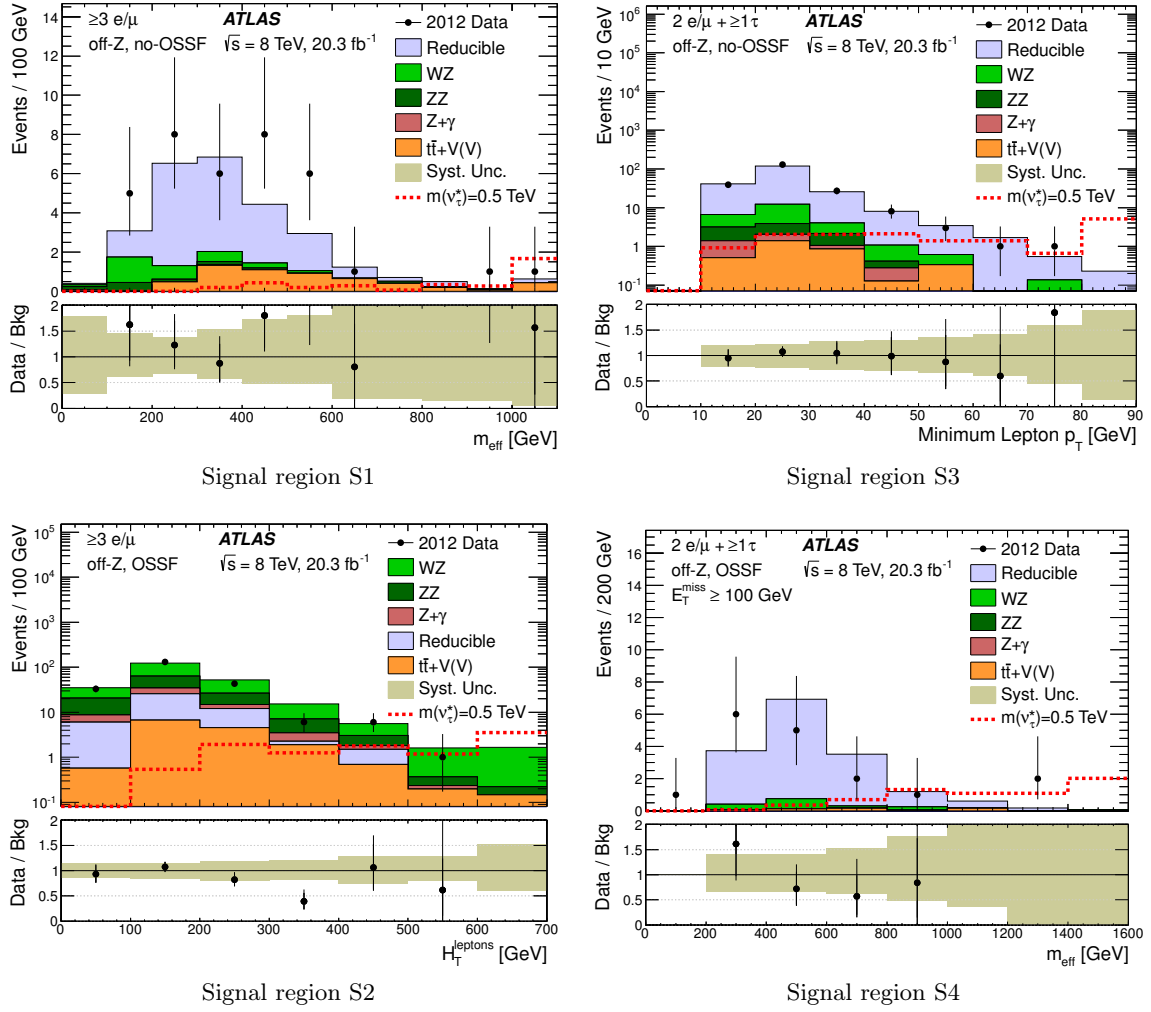


Figure 3: Data and background distributions of the ATLAS search analysis [98] used for reinterpretation in this work. The definition of the signal regions S1 ... S4 is given in Table 2. The data and background counts are explicitly listed in Table 4. Copyright 2018 CERN for the benefit of the ATLAS Collaboration. CC-BY-4.0 license

Depending on the signal region, different kinematic variables are used in the measurement:

- H_T^{leptons} : the scalar sum of p_T of the leptons used to categorise the event.
- **Minimum lepton p_T** : minimum lepton transverse momentum.
- m_{eff} : the effective mass of the event which combines the scalar sum of missing energy, scalar sum of the jets and the total p_T of the leptons in the event.

An overview of the signal regions and observables applied is provided in Table 2 and Table 3. The selection of histograms from [98] we reinterpret in this work are shown in Fig. 3¹⁰. As

¹⁰There are six histograms in total, we choose the four which are most constraining for our model.

	$\geq 3e/\mu$	$2e/\mu \geq 1\tau_{\text{had}}$
no OSSF	S1	S3
OSSF	S2	S4

Table 2: Signal regions. Note that S4 has an additional missing transverse energy requirement of at least 100 GeV.

Signal region	S1	S2	S3	S4
Observable	m_{eff}	H_T^{leptons}	Min. lepton p_T	m_{eff}

Table 3: Signal regions and observables used.

SR	Bin	N_{obs}	N_{BG}	ΔN_{BG}
S1	2	5	3.08	0.43
	3	8	6.52	0.91
	4	6	6.84	0.71
	5	8	4.44	0.53
	6	6	2.95	0.39
	7	1	1.24	0.11
SR	Bin	N_{obs}	N_{BG}	ΔN_{BG}
S2	1	33	35.35	4.92
	2	132	123.04	16.46
	3	43	52.17	6.79
	4	6	15.23	1.36
	5	6	5.64	0.65
	6	1	1.17	0.09
SR	Bin	N_{obs}	N_{BG}	ΔN_{BG}
S3	2	39	41.13	8.40
	3	129	119.82	18.95
	4	27	25.89	3.59
	5	8	8.08	1.05
	6	3	3.44	0.41
	7	1	1.67	0.21
	8	1	0.54	0.07
SR	Bin	N_{obs}	N_{BG}	ΔN_{BG}
S4	2	6	3.72	0.50
	3	5	6.93	0.87
	4	2	3.51	0.46
	5	1	1.19	0.15
	6	0	0.61	0.08
	7	2	0.17	0.03

Table 4: Observed (N_{obs}) and background (N_{BG}) counts reported by ATLAS for each signal region (SR) used in this analysis .

can be seen, the dominant SM processes which contribute to multi-leptonic final states are diboson production and production of a top quark pair in association with a weak gauge boson. The statistics associated to the m_{eff} kinematic variable are relatively low in comparison with the minimum lepton p_T and H_T^{leptons} . Although, there is generally good agreement between the SM predictions and the data; there are regions where the observed event yield is lower than the expected yield by more than three times the uncertainty on the expectation, and this occurs for the low statistics histograms.

3.5.3 Event Simulation and Analysis

The Universal FeynRules Output (UFO) for the model is generated using FeynRules [94]. The model information in the Universal FeynRules Output format is imported into the SHERPA event generator [95] to provide a full simulation of BSM processes at the particle level.

As the Higgs portal coupling, shown in Eq. (2.12), is the only way the flavons can be produced at a hadron collider, gluon fusion will be the most relevant production channel for the flavons. Although, BSM is available at next-to-leading order (NLO) accuracy in NLOCT prepackaged in FeynRules [105], this feature is currently not implemented in Sherpa. Therefore, we simply correct the tree-level cross sections with a K-factor of 2.2 for the BSM processes in this model [106]. This K-factor is computed at next-to-next-to leading order [107–109], for gluon fusion which is the dominant production mechanism of the Higgs [110]. As the flavons decay leptonically, additional radiations from the final states should not affect our results significantly. There are several kinematic regimes which are important for flavon production:

- $m_{s_i} < \frac{m_h}{2}$

In this kinematic regime, the flavons may be pair produced by the Higgs.

- $m_{s_i} < m_h$

The three-body decay $h_i \rightarrow s f \bar{f}$ is kinematically allowed, however this will be suppressed by phase space.

- $2m_h < m_{s_i}$

The pair production of the Higgs becomes kinematically accessible.

From Eq. (2.10), we observe that three-body decays of the scalars to scalar and two leptons are possible but they are expected to be subdominant due to phase space suppression. However, for certain points in the model parameter space, \mathbf{p} , it is possible that the three-body decays are non-negligible [92] and therefore are included in our Monte-Carlo simulations. The dominant configuration is two scalars in the final state where all possible combinations are generated. The subdominant contribution is one scalar in the final state with two leptons (both in charged lepton flavour conserving and violating combinations) as shown in Fig. 4. SHERPA uses the matrix element generator Comix [111] to find all contributing diagrams.

To summarise, for each test point \mathbf{p} we simulate 10^6 events¹¹ with SHERPA in a setup that includes the following processes:

- $pp \rightarrow s_i s_j$ where the flavons are denoted as s_i and s_j for $i, j = \{1, 2, 3\}$.
- $pp \rightarrow s_i \ell \bar{\ell}$ where s_i for $i = \{1, 2, 3\}$ and ℓ denotes the charged leptons.

¹¹The necessity for such a high number of generated signal events compared to the few hundreds of observed and background events comes from the relatively low tau-efficiencies.

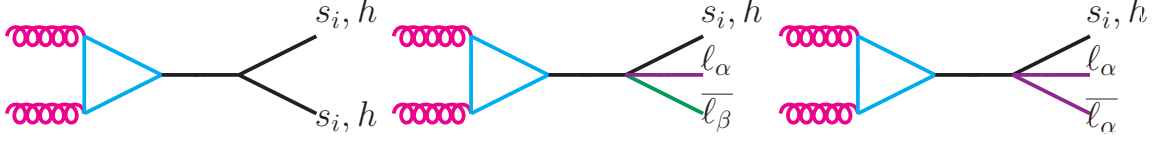


Figure 4: Flavon production channels.

The generated scalars are decayed according to internally calculated branching ratios. Furthermore, SHERPA takes care of QED and QCD radiation as well as hadronisation and effects such as hadron decays and multiple parton interactions. These events are then passed through the ATLAS analysis using RIVET and the output is a signal histogram of expected event yields for each \mathbf{p} that can be compared with data and background estimates since RIVET applies all relevant detector effects.

3.5.4 The CLs Method

In order to infer information on the viability of a given point \mathbf{p} , the expected event yield within the signal regions of the analysis is compared to the observed data and estimated backgrounds as reported by the collaboration on HepData [112]. As the experiment has not reported a discrepancy between data and the estimated backgrounds, we set an upper limit on the signal cross section normalised to the nominal cross section as calculated by SHERPA through frequentist interval estimation based on the *profile likelihood* [113]. In this model, the probability of observing data \mathcal{D} is a function of parameters that are grouped into two sets: the *parameters of interest* (POIs), in this case the normalised cross section μ , as well as *nuisance parameters* θ . The log-likelihood ratio is given by

$$\lambda(\mu) = \frac{p(\mu, \hat{\theta}|\mathcal{D})}{p(\hat{\mu}, \hat{\theta}|\mathcal{D})}, \quad (3.8)$$

where $\hat{\mu}$ and $\hat{\theta}$ are the best-fit value for an unconstrained fit of the model against the data and $\hat{\theta}$ are the best-fit values for the nuisance parameters for a constrained fit with a constant signal strength μ . We choose to use the reported per-bin uncertainty as a shape-systematic on the reported estimated background, such that the model has one nuisance parameter γ_i for each bin entering the fit.

In order to set an upper limit, we use the test statistic q_μ

$$q_\mu = \begin{cases} -2 \log \lambda(\mu) & \text{for } \hat{\mu} \leq \mu \\ 0 & \text{for } \hat{\mu} > \mu, \end{cases} \quad (3.9)$$

where the choice of test statistic is only dependent on the parameter of interest and avoids counting upward fluctuations in which the best fit value $\hat{\mu}$ exceeds the tested signal strength μ as evidence against signal hypothesis.

For the hypothesis test, we evaluate the modified p -value CL_s which is commonly used by collider experimentalists and is defined to be

Experimental data	Exclusion power[%]
MEG (Section 3.2)	65.6
ATLAS (Section 3.5)	40.0
Higgs-width (Section 3.4)	6.0
Higgs-mixing (Section 3.3)	1.7
$g - 2$ (Section 3.1)	0.7

Table 5: Exclusion power of constraints derived from experimental data.

$$\text{CL}_s(\mu) = \frac{\text{CL}_{s+b}}{\text{CL}_b} = \frac{\int_{q_{\mu,\text{obs}}}^{\infty} p(q_{\mu}|\mu' = \mu) dq_{\mu}}{\int_{q_{\mu,\text{obs}}}^{\infty} p(q_{\mu}|\mu' = 0) dq_{\mu}}, \quad (3.10)$$

in which $p(q_{\mu}|\mu')$ is the distribution of the test statistic q_{μ} for data, which is populated according to a signal strength μ' which we compute using the asymptotic formulae derived in [113]. To compute the CL_s values, the Python-based implementation of HistFactory [114] `pyhf` was applied [115].

Subsequently, generated signal points are assessed at nominal signal strength $\text{CL}_s = \text{CL}_s(\mu = 0)$ and points for which $\text{CL}_s < 0.05$ are considered to be excluded at 95% confidence level.

4 Results

The main results of this study are summarised in Table 5 and Table 6. As can be seen from Table 5, MEG excludes 65.6% of the total model parameter space, while the 8 TeV collider analysis excludes 40.0%. The constraints from Higgs measurements provide a total exclusionary power of 7.7% while the $g - 2$ experiment excludes the smallest volume of the parameter space.

In addition to schematically quantifying the exclusionary power of each measurement, we have demonstrated the *complementary* between the collider analysis and that of MEG. As detailed in Table 6, of the 3045 (34.8%) points which cannot be excluded by MEG, we found 378 of those points (12.4%) can be conservatively excluded by a combination of Higgs width, Higgs-scalar mixing and the ATLAS analysis. Moreover, of the 5317 (60.0%) points which are not excluded by the collider analysis, 2386 (44.87%) of those may be excluded by MEG. Interestingly, although the exclusionary power of the Higgs width and Higgs-scalar mixing is not considerable, when combined with the collider analysis, a sizeable portion of the parameter space which cannot be excluded by MEG becomes excluded. This is because the collider data is sensitive to the portal coupling of the flavons with the Higgs.

The exclusionary power of each experiment on the six-dimensional model parameter is presented in Figs. 5-10. These figures comprise of two types of plots: two-dimensional projections of the six-dimensional model parameter space and histograms for a single model parameter. In the histograms the yellow regions represents the model parameter subspaces which cannot be excluded by the relevant experiment while the dark blue denotes the

Constraint j \ Constraint i	MEG	ATLAS	H-width	H-mixing	$g - 2$
Number of points not excluded by i	3045	5317	8331	8710	8806
	of those, j excludes				
MEG	—	2386	5469	5746	5761
ATLAS	114	—	3164	3452	3489
H-width	183	150	—	490	523
H-mixing	81	59	111	—	155
$g - 2$	0	0	48	59	—
Number of points excluded by i	5820	3707	534	155	59
	of those, j excludes				
MEG	—	3434	351	74	59
ATLAS	3434	—	384	96	59
H-width	351	384	—	44	11
H-mixing	74	96	44	—	0
$g - 2$	59	59	11	0	—

Table 6: Summary table of exclusionary power for all 8865 points analysed. The table on top demonstrates the complementarity of e.g. MEG and ATLAS— of the 3045 points *not* excluded by MEG, the ATLAS data is able to exclude 114 points while MEG is able to exclude 2386 of the 5317 points *not* excluded by the ATLAS data. Similarly, the bottom table shows the overlap of exclusion of e.g. MEG and ATLAS— of the 5820 points excluded by MEG, the ATLAS data is able to exclude 3434 points.

regions which are excluded at 95% C.L. In the two-dimensional projection plots the colours have the same meaning (yellow to dark blue represents lesser to greater exclusionary power in those parameter space) but there is also additional information encoded in the size of the coloured dots: the larger the dot size the higher the density of sampled points in that region¹².

Fig. 5 shows the results using ATLAS data exclusively. We observe that for higher values of v_φ (the VEV of the flavons) the exclusionary power decreases. This is to be expected as the flavon masses increase with v_φ and therefore their production cross section decreases. However, for the majority of the model parameter space, $v_\varphi \lesssim 10^{2.0}$ GeV is excluded at 95% C.L. In the case of the cross-coupling between the flavons and the Higgs, ϵ , the smaller values ($\epsilon < 10^{-2}$) become increasingly more difficult to exclude. This is simply due to the fact that the production cross section of the flavons decreases for smaller values of ϵ . Moreover, we note that there is periodic behaviour in the polar coordinate, θ_φ .

¹²Some regions are more sparsely populated from as the six conditions on the sampling space (Section 3) can exclude more or less points in a given region of parameter space.

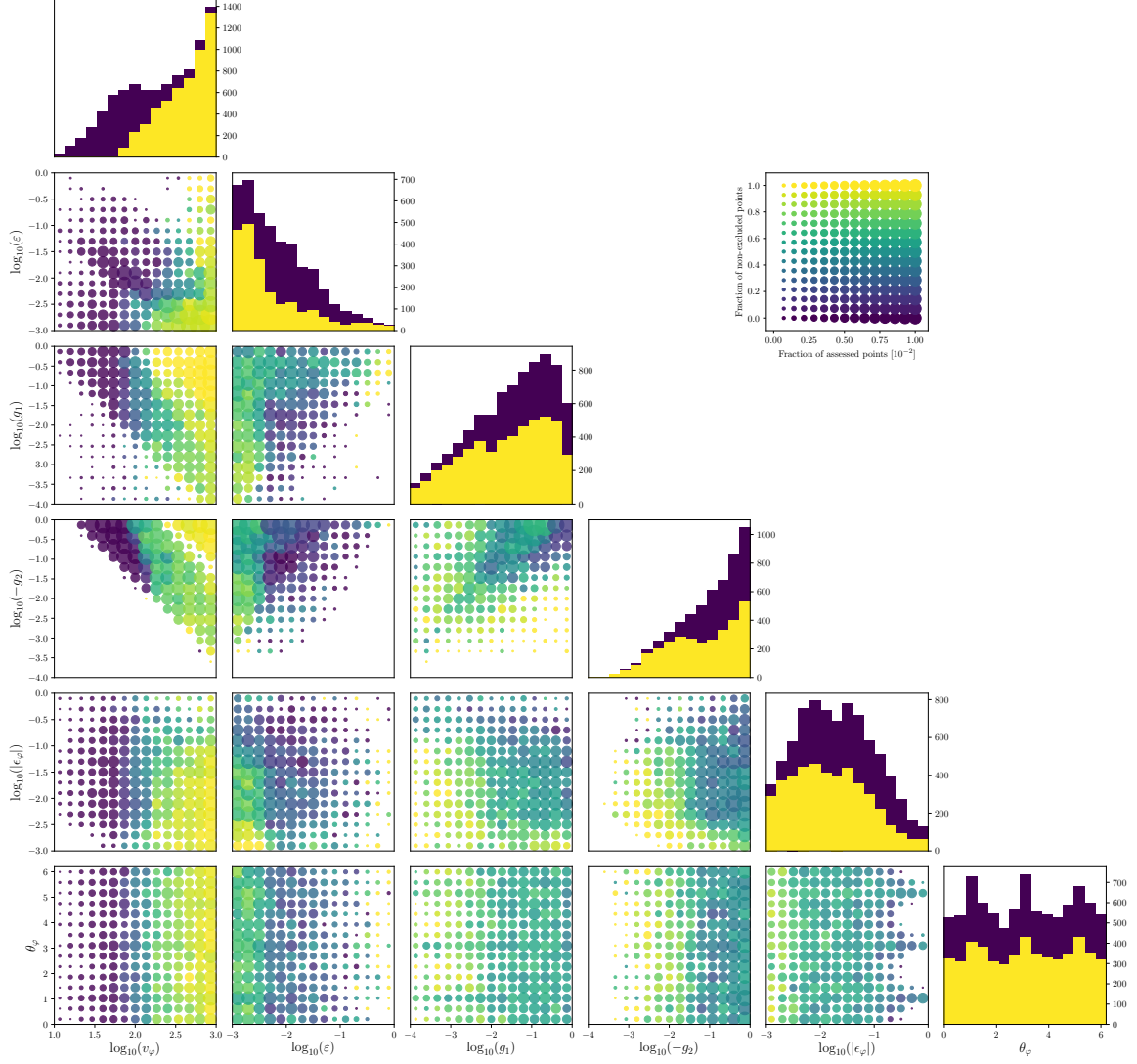


Figure 5: Results for ATLAS only. The histograms show the 1-dimensional projections of the number of excluded (purple) and not excluded (yellow) points. The scatter plots are a representation of 2-dimensional projections. The size of the circle indicates the fraction of the N_{tot} points analysed in a single bin while the colour shows what fraction of those points can be considered excluded.

We note that the excluded parameter-space constitutes an irregular body that does not align with the parameter axes. We therefore observe non-trivial correlations between the parameters when testing for compatibility with experimental observation. In an attempt to disentangle which parameters are dominantly probed by the ATLAS experiment we have plotted the regions of exclusion (for ATLAS) in which the points $v < 10^{1.8}$ GeV have been removed as shown in Fig. 6. From this figure, we observe that the shape of histograms for parameters ϵ and $|\epsilon_\varphi|$ changes relatively little after excluding the points for which $v_\varphi < 10^{1.8}$ GeV. This implies the ATLAS analysis has greatest sensitivity to these two parameters. In

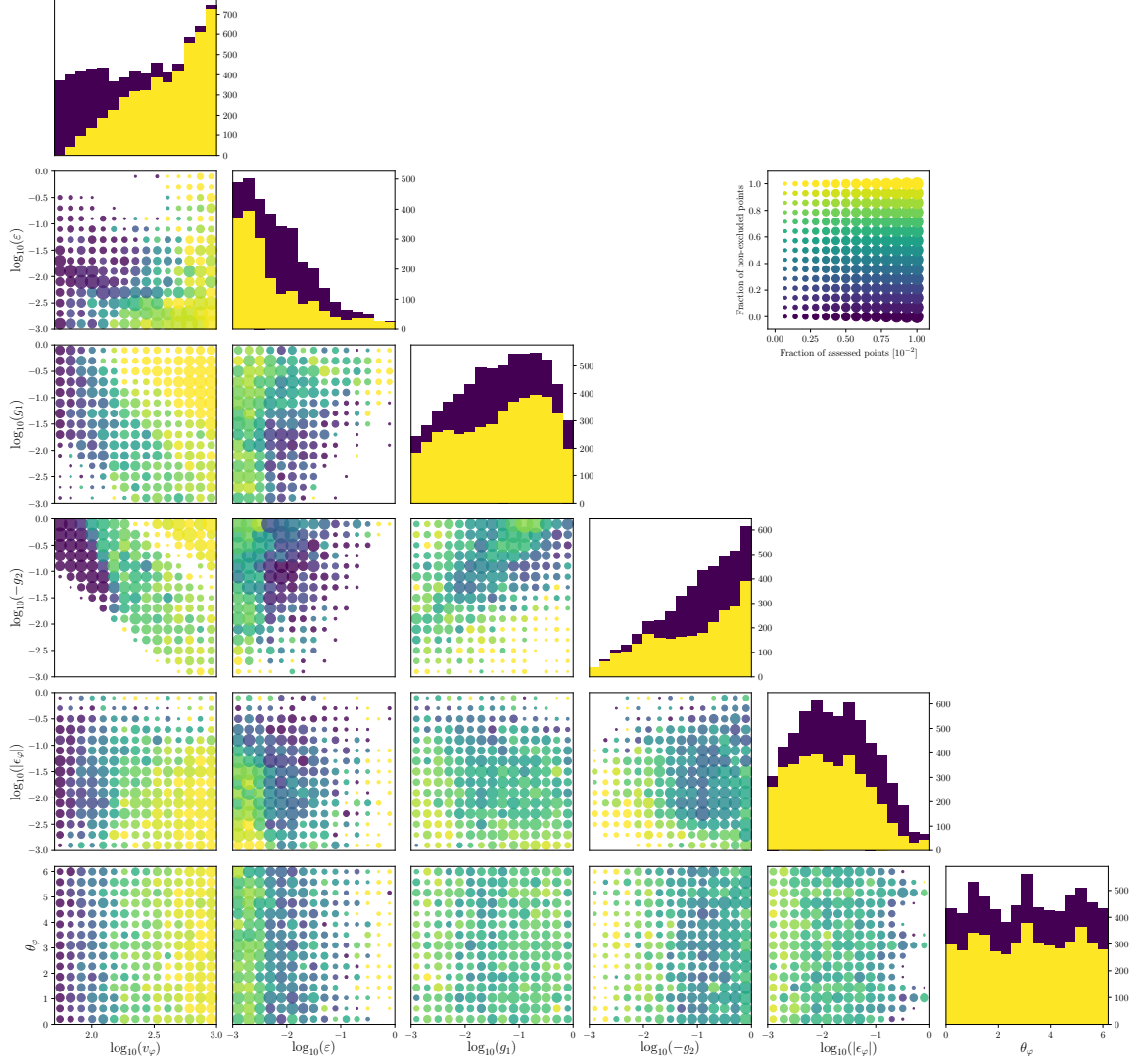


Figure 6: Results for ATLAS only excluding points for which $v_\varphi < 10^{1.8}$ GeV. As before the histograms show the 1-dimensional projections of the number of excluded (purple) and not excluded (yellow) points. The scatter plots are a representation of 2-dimensional projections.

terms of the former parameter, ϵ , this is the cross coupling of the flavons to the SM Higgs. As the flavon production is directly mediated via this coupling, this explains the sensitivity of this ATLAS search to ϵ . Moreover, as this ATLAS search looked for final states which violated charged lepton flavour this analysis has sensitivity to $|\epsilon_\varphi|$.

The exclusion from MEG alone is shown in Fig. 7. It can be observed that the exclusionary power on v_φ , which is the parameter that encapsulates the flavour breaking scale, is greater than that of ATLAS alone and that $v_\varphi \lesssim 10^{2.0}$ GeV is excluded at 95% C.L. Moreover, the cross-coupling is particularly constrained to a corner of the parameter space, $\epsilon < 10^{-2.5}$. We note that the constraints on g_1 and g_2 are much more aggressive compared

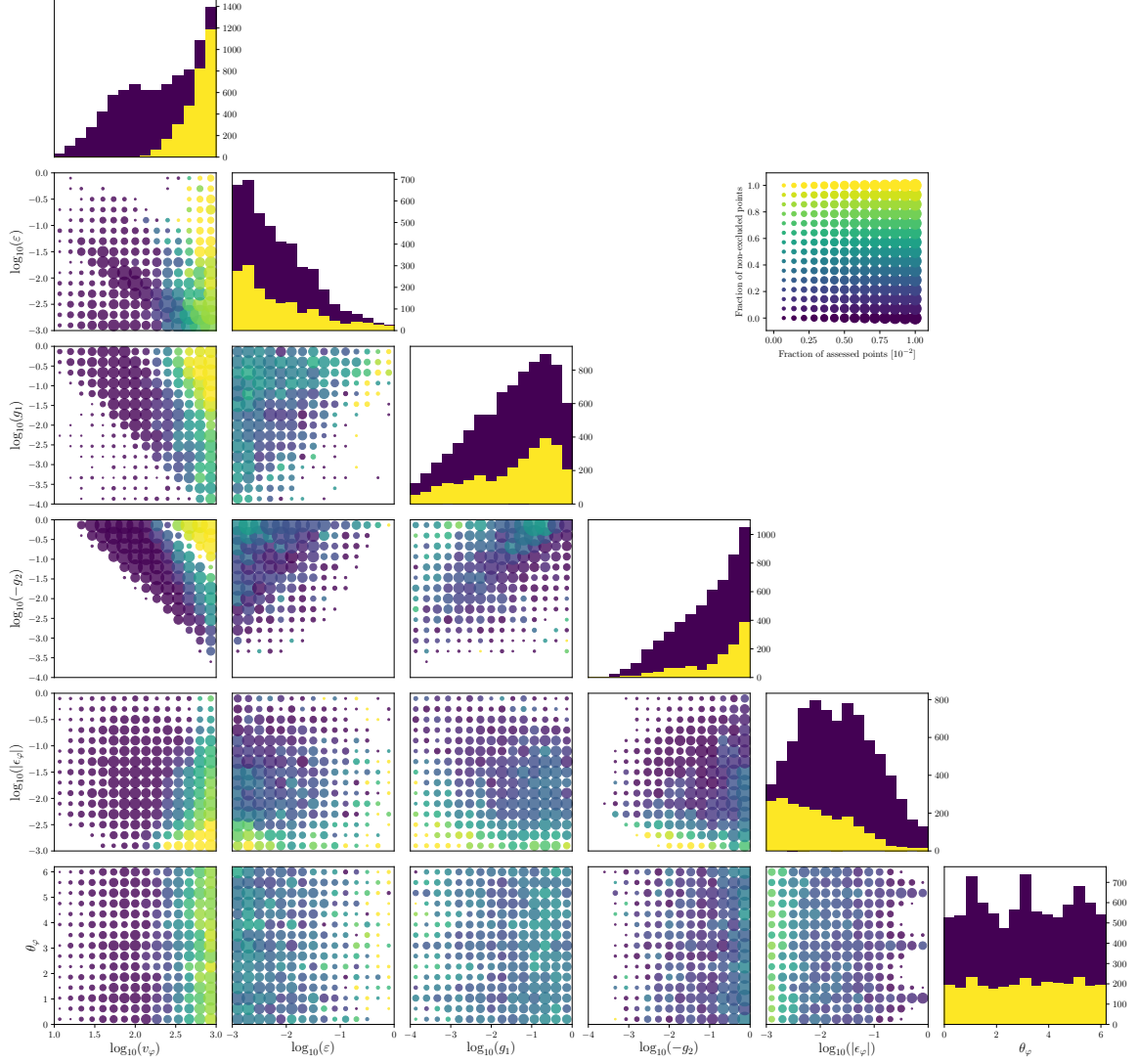


Figure 7: Results for MEG only. The histograms show the 1-dimensional projections of the number of excluded (purple) and not excluded (yellow) points. The scatter plots are a representation of 2-dimensional projections. The size of the circle indicates the fraction of the N_{tot} points analysed in a single bin while the colour shows what fraction of those points can be considered excluded.

to the constraint from ATLAS.

As there are non-trivial correlations between the parameters of the model, in order to disentangle the impact of v_φ , we show the same plot as Fig. 7 but with the points $v_\varphi < 10^{2.0}$ GeV excluded in Fig. 8. In general, the shape of the histograms of the other five variables changes slightly. However, the histograms which change least in shape indicate which parameters are relatively independent of v_φ . Qualitatively, we find that the structure of the histogram of $|\epsilon_\varphi|$ changes the least which implies MEG has sensitivity to this parameters in addition to that of v_φ . We note that the shape of the other histograms for parameters g_1 ,

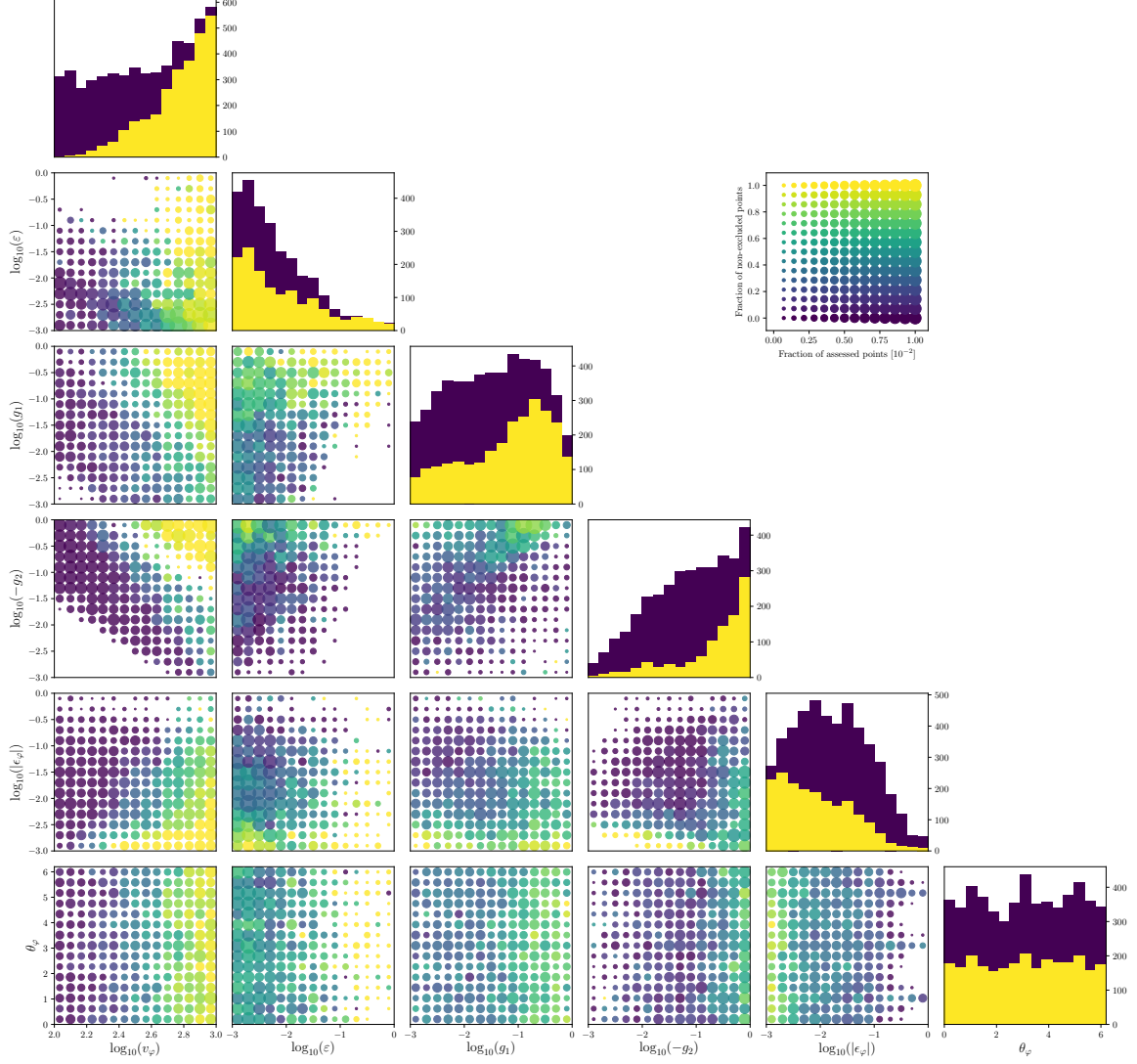


Figure 8: Results for MEG only excluding points for which $v_\varphi < 10^{2.0}$ GeV. The histograms show the 1-dimensional projections of the number of excluded (purple) and not excluded (yellow) points. The scatter plots are a representation of 2-dimensional projections. The size of the circle indicates the fraction of the N_{tot} points analysed in a single bin while the colour shows what fraction of those points can be considered excluded.

g_2 , θ_φ and ϵ all change significantly. This implies the exclusionary power of MEG in those parameters is correlated with v_φ . It is unsurprising that MEG has sensitivity to $|\epsilon_\varphi|$ as the very CLFV nature of this model is parametrised by this variable.

The plot in Fig. 9 shows the combined MEG and ATLAS constraints. Finally, Fig. 10 shows the constraints from all included experimental data. We find that there is not a significant qualitative difference between the two plots (as the Higgs and $g - 2$ constraints are very weak). We observe that the flavour breaking scale, parametrised by v_φ , must be greater than $\sim 10^{2.5}$ GeV. Moreover, the cross-coupling between this flavour sector and

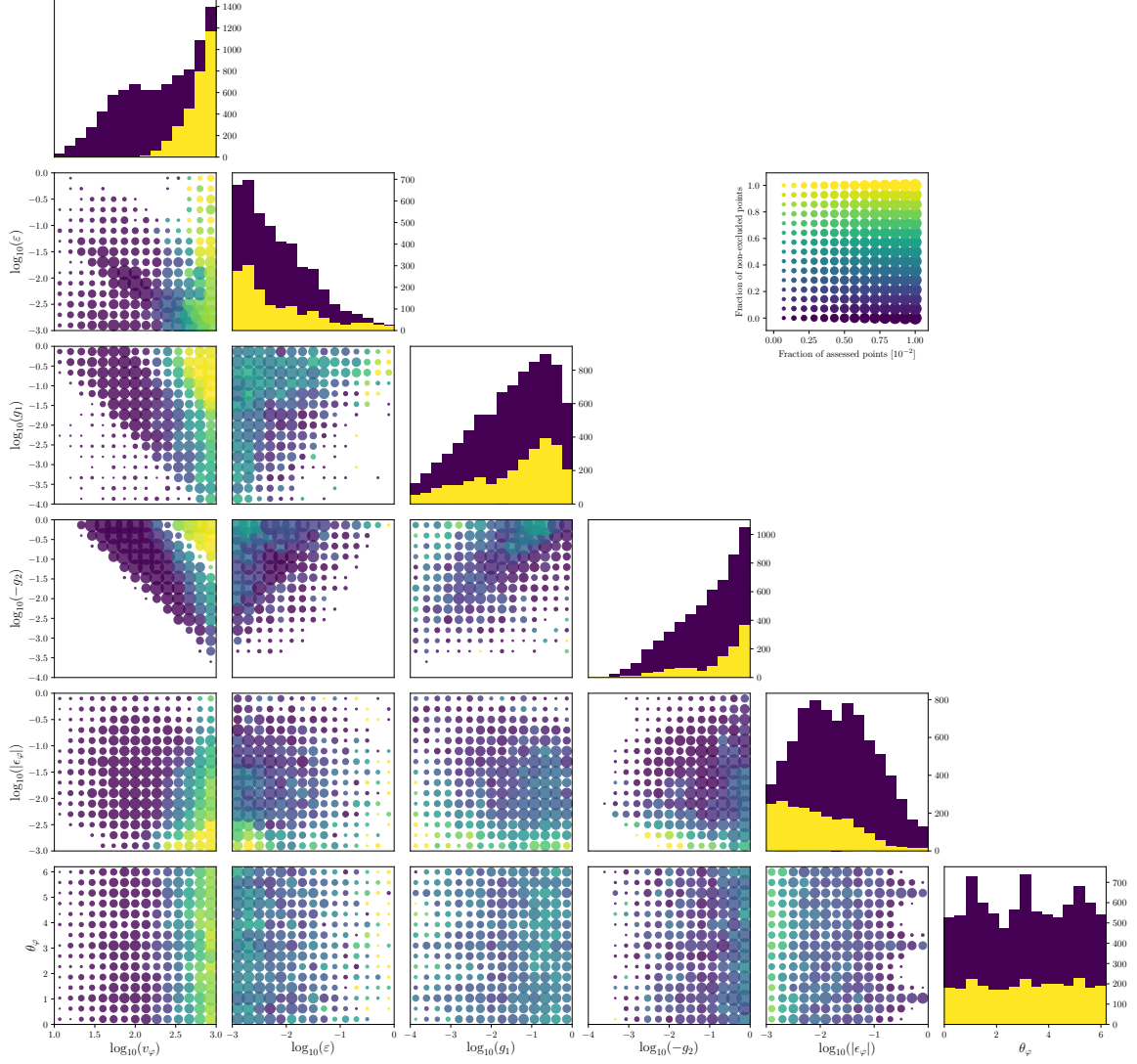


Figure 9: Results for MEG and ATLAS combined. The histograms show the 1-dimensional projections of the number of excluded (purple) and not excluded (yellow) points. The scatter plots are a representation of 2-dimensional projections. The size of the circle indicates the fraction of the N_{tot} points analysed in a single bin while the colour shows what fraction of those points can be considered excluded.

the SM must be $\epsilon < 10^{-2}$. The absolute value of the parameter which controls how much the residual \mathbb{Z}_3 symmetry of the charged lepton sector is broken, is particularly constrained $|\epsilon_\varphi| < 10^{-2.75}$ ¹³. However, the polar coordinate of the \mathbb{Z}_3 -breaking parameter is constrained to $\theta_\varphi < 0.5$ radians. In summary, the majority of the chosen model parameter space can be excluded through the combination of the measurements from the ATLAS analysis, MEG, $g - 2$ experiments and Higgs measurement data.

¹³We note that this statement naturally depends on the specific point in the model parameter space.

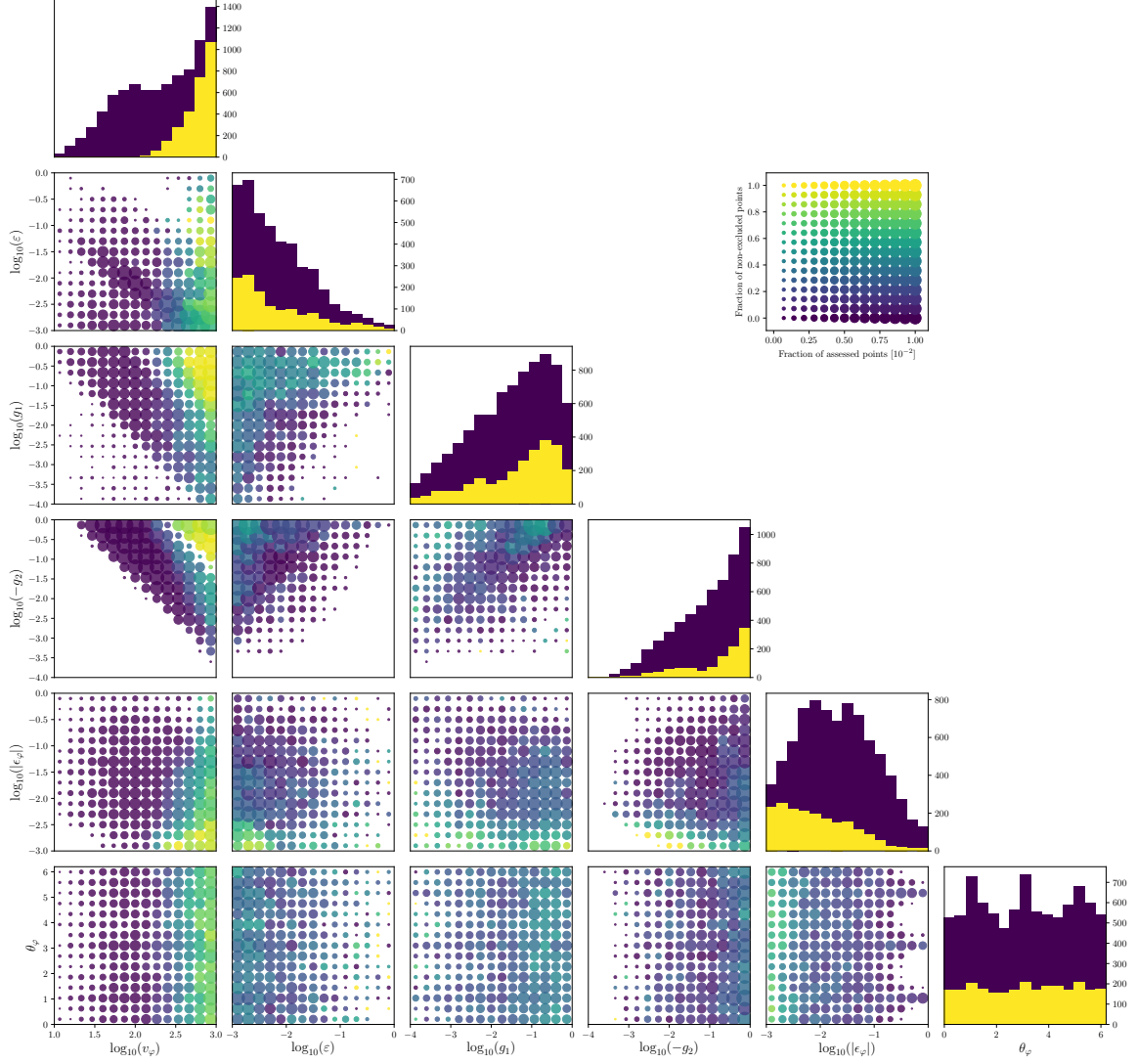


Figure 10: Results using all data constraints. The histograms show the 1-dimensional projections of the number of excluded (purple) and not excluded (yellow) points. The scatter plots are a representation of 2-dimensional projections. The size of the circle indicates the fraction of the N_{tot} points analysed in a single bin while the colour shows what fraction of those points can be considered excluded.

5 Summary

Explaining the origin of the flavour structure, in both quark and lepton sectors, has been a recurring theme in many proposed extensions of the SM. One such approach to explain the pattern of leptonic mixing is the application of discrete, non-Abelian flavour symmetries. This flavour symmetry must be broken in the low-energy effective theory but its residual symmetries survive and play an important role in predicting the structure of the leptonic mixing matrix.

In this work, we did not presuppose the flavour breaking scale was high (close to the

GUT scale) and therefore it is an interesting endeavour to constrain this flavour model's parameter space using a synergy of experimental data. In order to exclude regions of the model parameter space, we applied constraints from $g - 2$, MEG, Higgs-scalar mixing and Higgs width measurements. In addition, we recasted an 8 TeV ATLAS analysis which searched for events with high-multiplicities of leptonic final states. We believe we are the first to combine, in both a conservative and rigorous manner, such experimental data to constrain a leptonic flavour model.

One of our primary aims was to be as generic as possible in constraining the parameter space of a well-motivated flavour model, such as A_4 . Therefore, we chose to investigate a simplified description of an A_4 model. At leading order this model has the general features of most A_4 models, where the residual symmetry \mathbb{Z}_3 (\mathbb{Z}_2) is preserved in the charged lepton (neutrino) sector and consequently TBM mixing is predicted after A_4 symmetry breaking. However, at sub-leading order, the residual symmetries are slightly broken due to the shift in one of the flavon VEVs. As a consequence, a pattern of mixing consistent with neutrino oscillation data is achieved. We mainly focus on the phenomenology of the flavon, φ which couples to charged leptons as it has greater experimental visibility than its neutrino flavon counterpart, χ .

We conducted an exploration of the six-dimensional model parameter space and found most of the constraints could be calculated analytically. The collider reinterpretation of an 8 TeV ATLAS measurement was a more involved process. We benefited greatly from the ATLAS collaboration both preserving and validating their analysis; moreover, the analysis was publicly available via RIVET which we used as our analysis tool. We believe we are the first to utilise the Monte-Carlo event generator, SHERPA, for BSM purposes, which was particularly amenable as the fully-showered and hadronised Monte-Carlo events could directly be fed into the analysis tool. Although we focused on an economical model, most basic features of leptonic flavour models have been included, e.g., interactions related to lepton mass generation, interactions leading to the breaking of flavour symmetry and residual symmetries, as well as the Higgs-portal interactions. An alternative model may increase the number of free parameters but preserve most of these features and this investigation remain relevant.

We found the most aggressive constraints derived from the CLFV limit set by the MEG experiment; approximately $\sim 60\%$ of the parameter space could be excluded. The exclusionary power exhibited by the ATLAS analysis came second only to MEG; excluding $\sim 40\%$. The remaining experimental data had smaller but non-negligible exclusionary power. Interestingly, the exclusionary power of MEG and the collider experimental data complement each other: the collider analysis, combined with Higgs width and Higgs-scalar mixing constraints, can exclude regions MEG simply cannot and vice versa. This is because the collider search is sensitive to the mixing of the flavons with the SM Higgs doublet, while the constraints from MEG is not.

We hope the collider experimentalists view this optimistically, that searches for high-multiplicity leptonic final states exclude sizeable regions of the leptonic flavour model parameter space and complement limits set by experiments dedicated to searching for CLFV. Moreover, at higher centre of mass energies, the exclusionary power of collider searches for

anomalous production of leptonic final states may seriously compete with those of MEG. Work to precisely quantify this statement is of interest but relegated for future studies. In addition, the construction and optimisation of an analysis for final states such as $\tau\tau\mu e$, which would be a useful step in constraining the flavour breaking scale, if indeed such a scale exists.

Acknowledgments

We would like to thank Bogdan Dobrescu for helpful advice throughout and proofreading this manuscript. We are grateful to Beate Heinemann and Mike Hance for useful advice regarding the reinterpretation of ATLAS analysis presented in [98]. It is a pleasure to thank Silvan Kuttimalai on helpful discussions regarding Sherpa. We would like to thank Zhen Liu, Serguey Petcov and Alexis Plascencia for helpful conversations about various aspects of this work. L.H. is supported through NSF ACI-1450310 and PHY-1505463. This manuscript has been authored by Fermi Research Alliance, LLC under Contract No. DE-AC02-07CH11359 with the U.S. Department of Energy, Office of Science, Office of High Energy Physics. This material is based upon work supported by the U.S. Department of Energy, Office of Science, Office of Advanced Scientific Computing Research, Scientific Discovery through Advanced Computing (SciDAC) program. Y.L.Z. acknowledges the STFC Consolidated Grant ST/L000296/1 and the European Union’s Horizon 2020 Research and Innovation programme under Marie Skłodowska-Curie grant agreements Elusives ITN No. 674896 and InvisiblesPlus RISE No. 690575.

A Group Theory for A_4

In this paper, as in [62], we work in the Altarelli-Feruglio basis [14], where T is diagonal. T and S are respectively given by

$$T = \begin{pmatrix} 1 & 0 & 0 \\ 0 & \omega^2 & 0 \\ 0 & 0 & \omega \end{pmatrix}, \quad S = \frac{1}{3} \begin{pmatrix} -1 & 2 & 2 \\ 2 & -1 & 2 \\ 2 & 2 & -1 \end{pmatrix}. \quad (\text{A.1})$$

The products of two 3-dimensional irreducible representations $a = (a_1, a_2, a_3)^T$ and $b = (b_1, b_2, b_3)^T$ can be expressed as

$$\begin{aligned} (ab)_{\mathbf{1}} &= a_1 b_1 + a_2 b_3 + a_3 b_2 \\ (ab)_{\mathbf{1}'} &= a_3 b_3 + a_1 b_2 + a_2 b_1 \\ (ab)_{\mathbf{1}''} &= a_2 b_2 + a_1 b_3 + a_3 b_1 \\ (ab)_{\mathbf{3}_S} &= \frac{1}{2} \begin{pmatrix} 2a_1 b_1 - a_2 b_3 - a_3 b_2 \\ 2a_3 b_3 - a_1 b_2 - a_2 b_1 \\ 2a_2 b_2 - a_3 b_1 - a_1 b_3 \end{pmatrix}, \quad (ab)_{\mathbf{3}_A} = \frac{1}{2} \begin{pmatrix} a_2 b_3 - a_3 b_2 \\ a_1 b_2 - a_2 b_1 \\ a_3 b_1 - a_1 b_3 \end{pmatrix}. \end{aligned} \quad (\text{A.2})$$

B Higgs Width Constraint

In this Appendix, we provide the coupling of the Higgs to the flavon mass eigenstates and detail how the SM Higgs width is calculated from such coupling. As introduced in Section 2.2, the gauge and mass eigenstates of the scalar sector in the \mathbb{Z}_3 -breaking scenario, may be related by the unitary matrix

$$\begin{pmatrix} \tilde{h} \\ \tilde{\varphi}_1 \\ \sqrt{2}\text{Re}(\varphi_2) \\ \sqrt{2}\text{Im}(\varphi_2) \end{pmatrix} = \begin{pmatrix} W_{00} & W_{01} & W_{02} & W_{03} \\ W_{10} & W_{11} & W_{12} & W_{13} \\ W_{20} & W_{21} & W_{22} & W_{23} \\ W_{30} & W_{31} & W_{32} & W_{33} \end{pmatrix} \begin{pmatrix} h \\ s_1 \\ s_2 \\ s_3 \end{pmatrix}.$$

Using the above notation, the \mathbb{Z}_3 -breaking triplet couplings are given below

$$\begin{aligned} \tilde{g}_{hs_1^2} &= g_2 v_\varphi W_{10} W_{11}^2 - \frac{1}{2} g_2 v_\varphi W_{20} W_{21}^2 - \frac{1}{2} g_2 v_\varphi W_{30} W_{31}^2 - \frac{1}{2} g_2 \epsilon_\varphi v_\varphi W_{10} W_{21}^2 \\ &\quad - g_2 \epsilon_\varphi v_\varphi W_{11} W_{20} W_{21} + 3g_2 \epsilon_\varphi v_\varphi W_{20} W_{21}^2 - \frac{1}{2} g_2 \epsilon_\varphi^* v_\varphi W_{10} W_{31}^2 - g_2 \epsilon_\varphi^* v_\varphi W_{11} W_{30} W_{31} \\ &\quad + 3\lambda v_H W_{00} W_{01}^2 + \frac{1}{2} v_H W_{00} W_{11}^2 \epsilon + v_H W_{00} W_{21} W_{31} \epsilon + v_H W_{01} W_{10} W_{11} \epsilon \\ &\quad + v_H W_{01} W_{20} W_{31} \epsilon + v_H W_{01} W_{21} W_{30} \epsilon + v_\varphi W_{00} W_{01} W_{11} \epsilon + \frac{1}{2} v_\varphi W_{01}^2 W_{10} \epsilon \\ &\quad + \epsilon_\varphi v_\varphi W_{00} W_{01} W_{31} \epsilon + \frac{1}{2} \epsilon_\varphi v_\varphi W_{01}^2 W_{30} \epsilon + \epsilon_\varphi^* v_\varphi W_{00} W_{01} W_{21} \epsilon + \frac{1}{2} \epsilon_\varphi^* v_\varphi W_{01}^2 W_{20} \epsilon, \end{aligned} \quad (\text{B.1})$$

$$\begin{aligned}
\tilde{g}_{hs_2^2} = & g_2 v_\varphi W_{10} W_{12}^2 - \frac{1}{2} g_2 v_\varphi W_{20} W_{22}^2 - \frac{1}{2} g_2 v_\varphi W_{30} W_{32}^2 - \frac{1}{2} g_2 \epsilon_\varphi v_\varphi W_{10} W_{22}^2 \\
& - g_2 \epsilon_\varphi v_\varphi W_{12} W_{20} W_{22} + 3 g_2 \epsilon_\varphi v_\varphi W_{20} W_{22}^2 - \frac{1}{2} g_2 \epsilon_\varphi^* v_\varphi W_{10} W_{32}^2 - g_2 \epsilon_\varphi^* v_\varphi W_{12} W_{30} W_{32} \\
& + 3 \lambda v_H W_{00} W_{02}^2 + \frac{1}{2} v_H W_{00} W_{12}^2 \epsilon + v_H W_{00} W_{22} W_{32} \epsilon + v_H W_{02} W_{10} W_{12} \epsilon \\
& + v_H W_{02} W_{20} W_{32} \epsilon + v_H W_{02} W_{22} W_{30} \epsilon + v_\varphi W_{00} W_{02} W_{12} \epsilon + \frac{1}{2} v_\varphi W_{02}^2 W_{10} \epsilon \\
& + \epsilon_\varphi v_\varphi W_{00} W_{02} W_{32} \epsilon + \frac{1}{2} \epsilon_\varphi v_\varphi W_{02}^2 W_{30} \epsilon + \epsilon_\varphi^* v_\varphi W_{00} W_{02} W_{22} \epsilon + \frac{1}{2} \epsilon_\varphi^* v_\varphi W_{02}^2 W_{20} \epsilon,
\end{aligned} \tag{B.2}$$

$$\begin{aligned}
\tilde{g}_{hs_3^2} = & g_2 v_\varphi W_{10} W_{13}^2 - \frac{1}{2} g_2 v_\varphi W_{20} W_{23}^2 - \frac{1}{2} g_2 v_\varphi W_{30} W_{33}^2 - \frac{1}{2} g_2 \epsilon_\varphi v_\varphi W_{10} W_{23}^2 \\
& - g_2 \epsilon_\varphi v_\varphi W_{13} W_{20} W_{23} + 3 g_2 \epsilon_\varphi v_\varphi W_{20} W_{23}^2 - \frac{1}{2} g_2 \epsilon_\varphi^* v_\varphi W_{10} W_{33}^2 - g_2 \epsilon_\varphi^* v_\varphi W_{13} W_{30} W_{33} \\
& + 3 \lambda v_H W_{00} W_{03}^2 + \frac{1}{2} v_H W_{00} W_{13}^2 \epsilon + v_H W_{00} W_{23} W_{33} \epsilon + v_H W_{03} W_{10} W_{13} \epsilon \\
& + v_H W_{03} W_{20} W_{33} \epsilon + v_H W_{03} W_{23} W_{30} \epsilon + v_\varphi W_{00} W_{03} W_{13} \epsilon + \frac{1}{2} v_\varphi W_{03}^2 W_{10} \epsilon \\
& + \epsilon_\varphi v_\varphi W_{00} W_{03} W_{33} \epsilon + \frac{1}{2} \epsilon_\varphi v_\varphi W_{03}^2 W_{30} \epsilon + \epsilon_\varphi^* v_\varphi W_{00} W_{03} W_{23} \epsilon + \frac{1}{2} \epsilon_\varphi^* v_\varphi W_{03}^2 W_{20} \epsilon,
\end{aligned} \tag{B.3}$$

$$\begin{aligned}
\tilde{g}_{hs_1 s_2} = & 2 g_2 v_\varphi W_{10} W_{11} W_{12} - g_2 v_\varphi W_{20} W_{21} W_{22} - g_2 v_\varphi W_{30} W_{31} W_{32} - g_2 \epsilon_\varphi v_\varphi W_{10} W_{21} W_{22} \\
& - g_2 \epsilon_\varphi v_\varphi W_{11} W_{20} W_{22} - g_2 \epsilon_\varphi v_\varphi W_{12} W_{20} W_{21} + 6 g_2 \epsilon_\varphi v_\varphi W_{20} W_{21} W_{22} - g_2 \epsilon_\varphi^* v_\varphi W_{10} W_{31} W_{32} \\
& - g_2 \epsilon_\varphi^* v_\varphi W_{11} W_{30} W_{32} - g_2 \epsilon_\varphi^* v_\varphi W_{12} W_{30} W_{31} + 6 \lambda v_H W_{00} W_{01} W_{02} + v_H W_{00} W_{11} W_{12} \epsilon \\
& + v_H W_{00} W_{21} W_{32} \epsilon + v_H W_{00} W_{22} W_{31} \epsilon + v_H W_{01} W_{10} W_{12} \epsilon + v_H W_{01} W_{20} W_{32} \epsilon \\
& + v_H W_{01} W_{22} W_{30} \epsilon + v_H W_{02} W_{10} W_{11} \epsilon + v_H W_{02} W_{20} W_{31} \epsilon + v_H W_{02} W_{21} W_{30} \epsilon \\
& + v_\varphi W_{00} W_{01} W_{12} \epsilon + v_\varphi W_{00} W_{02} W_{11} \epsilon + v_\varphi W_{01} W_{02} W_{10} \epsilon + \epsilon_\varphi v_\varphi W_{00} W_{01} W_{32} \epsilon \\
& + \epsilon_\varphi v_\varphi W_{00} W_{02} W_{31} \epsilon + \epsilon_\varphi v_\varphi W_{01} W_{02} W_{30} \epsilon + \epsilon_\varphi^* v_\varphi W_{00} W_{01} W_{22} \epsilon + \epsilon_\varphi^* v_\varphi W_{00} W_{02} W_{21} \epsilon \\
& + \epsilon_\varphi^* v_\varphi W_{01} W_{02} W_{20} \epsilon,
\end{aligned} \tag{B.4}$$

$$\begin{aligned}
\tilde{g}_{hs_1 s_3} = & 2 g_2 v_\varphi W_{10} W_{11} W_{13} - g_2 v_\varphi W_{20} W_{21} W_{23} - g_2 v_\varphi W_{30} W_{31} W_{33} - g_2 \epsilon_\varphi v_\varphi W_{10} W_{21} W_{23} \\
& - g_2 \epsilon_\varphi v_\varphi W_{11} W_{20} W_{23} - g_2 \epsilon_\varphi v_\varphi W_{13} W_{20} W_{21} + 6 g_2 \epsilon_\varphi v_\varphi W_{20} W_{21} W_{23} - g_2 \epsilon_\varphi^* v_\varphi W_{10} W_{31} W_{33} \\
& - g_2 \epsilon_\varphi^* v_\varphi W_{11} W_{30} W_{33} - g_2 \epsilon_\varphi^* v_\varphi W_{13} W_{30} W_{31} + 6 \lambda v_H W_{00} W_{01} W_{03} + v_H W_{00} W_{11} W_{13} \epsilon \\
& + v_H W_{00} W_{21} W_{33} \epsilon + v_H W_{00} W_{23} W_{31} \epsilon + v_H W_{01} W_{10} W_{13} \epsilon + v_H W_{01} W_{20} W_{33} \epsilon \\
& + v_H W_{01} W_{23} W_{30} \epsilon + v_H W_{03} W_{10} W_{11} \epsilon + v_H W_{03} W_{20} W_{31} \epsilon + v_H W_{03} W_{21} W_{30} \epsilon \\
& + v_\varphi W_{00} W_{01} W_{13} \epsilon + v_\varphi W_{00} W_{03} W_{11} \epsilon + v_\varphi W_{01} W_{03} W_{10} \epsilon + \epsilon_\varphi v_\varphi W_{00} W_{01} W_{33} \epsilon \\
& + \epsilon_\varphi v_\varphi W_{00} W_{03} W_{31} \epsilon + \epsilon_\varphi v_\varphi W_{01} W_{03} W_{30} \epsilon + \epsilon_\varphi^* v_\varphi W_{00} W_{01} W_{23} \epsilon + \epsilon_\varphi^* v_\varphi W_{00} W_{03} W_{21} \epsilon \\
& + \epsilon_\varphi^* v_\varphi W_{01} W_{03} W_{20} \epsilon,
\end{aligned} \tag{B.5}$$

$$\begin{aligned}
\tilde{g}_{hs_2s_3} = & 2g_2v_\varphi W_{10}W_{12}W_{13} - g_2v_\varphi W_{20}W_{22}W_{23} - g_2v_\varphi W_{30}W_{32}W_{33} - g_2\epsilon_\varphi v_\varphi W_{10}W_{22}W_{23} \\
& - g_2\epsilon_\varphi v_\varphi W_{12}W_{20}W_{23} - g_2\epsilon_\varphi v_\varphi W_{13}W_{20}W_{22} + 6g_2\epsilon_\varphi v_\varphi W_{20}W_{22}W_{23} - g_2\epsilon_\varphi^* v_\varphi W_{10}W_{32}W_{33} \\
& - g_2\epsilon_\varphi^* v_\varphi W_{12}W_{30}W_{33} - g_2\epsilon_\varphi^* v_\varphi W_{13}W_{30}W_{32} + 6\lambda v_H W_{00}W_{02}W_{03} + v_H W_{00}W_{12}W_{13}\epsilon \\
& + v_H W_{00}W_{22}W_{33}\epsilon + v_H W_{00}W_{23}W_{32}\epsilon + v_H W_{02}W_{10}W_{13}\epsilon + v_H W_{02}W_{20}W_{33}\epsilon \\
& + v_H W_{02}W_{23}W_{30}\epsilon + v_H W_{03}W_{10}W_{12}\epsilon + v_H W_{03}W_{20}W_{32}\epsilon + v_H W_{03}W_{22}W_{30}\epsilon \\
& + v_\varphi W_{00}W_{02}W_{13}\epsilon + v_\varphi W_{00}W_{03}W_{12}\epsilon + v_\varphi W_{02}W_{03}W_{10}\epsilon + \epsilon_\varphi v_\varphi W_{00}W_{02}W_{33}\epsilon \\
& + \epsilon_\varphi v_\varphi W_{00}W_{03}W_{32}\epsilon + \epsilon_\varphi v_\varphi W_{02}W_{03}W_{30}\epsilon + \epsilon_\varphi^* v_\varphi W_{00}W_{02}W_{23}\epsilon + \epsilon_\varphi^* v_\varphi W_{00}W_{03}W_{22}\epsilon \\
& + \epsilon_\varphi^* v_\varphi W_{02}W_{03}W_{20}\epsilon.
\end{aligned} \tag{B.6}$$

In comparison with the \mathbb{Z}_3 preserving scenario, this case has a larger number of possible mass combinations which may alter the Higgs total width. This is because the Higgs can decay to three distinct flavons with possible mixtures of flavons in the final state. In the scenario, a single scalar contributes to the Higgs width, $m_{s_i} < m_H/2$ with $i = 1, 2, 3$ and this implies

$$\Gamma(h \rightarrow s_i s_i) \leq 18 \text{ MeV}.$$

In the possibility of two scalars are lighter than half the mass of the Higgs, $m_i < m_H/2$ with $i = 1, 2, 3$ then the

- $m_i < m_H/2$ with $i = 1, 2, 3$

$$\Gamma(h \rightarrow s_i s_i) \leq 18 \text{ MeV}$$

- $m_i, m_j < m_H/2$ with $i, j = 1, 2, 3$

$$\Gamma(h \rightarrow s_i s_i) + \Gamma(h \rightarrow s_j s_j) + \Gamma(h \rightarrow s_i s_j) \leq 18 \text{ MeV}$$

- $m_i, m_j, m_k < m_H/2$ with $i, j, k = 1, 2, 3$

$$\Gamma(h \rightarrow s_i s_i) + \Gamma(h \rightarrow s_j s_j) + \Gamma(h \rightarrow s_k s_k) + \Gamma(h \rightarrow s_i s_j) + \Gamma(h \rightarrow s_i s_k) + \Gamma(h \rightarrow s_j s_k) \leq 18 \text{ MeV}$$

where

$$\Gamma(h \rightarrow s_i s_i) = \frac{\tilde{g}_{hs_i^2}}{8\pi m_h} \left(1 - \frac{4m_{s_i}^2}{m_h^2}\right)^{\frac{1}{2}} \quad \text{and} \quad \Gamma(h \rightarrow s_i s_j) = \frac{|p^*|}{2\pi m_h^2} g_{hs_i s_j}^2$$

with

$$|p^*| = \frac{1}{2m_H} \sqrt{\left[m_H^2 - (m_i + m_j)^2\right] \left[m_H^2 - (m_i - m_j)^2\right]}$$

References

- [1] SUPER-KAMIOKANDE collaboration, Y. Fukuda et al., *Evidence for oscillation of atmospheric neutrinos*, *Phys. Rev. Lett.* **81** (1998) 1562–1567, [[hep-ex/9807003](#)].

- [2] HYPER-KAMIOKANDE WORKING GROUP collaboration, K. Abe et al., *A Long Baseline Neutrino Oscillation Experiment Using J-PARC Neutrino Beam and Hyper-Kamiokande*, 2014, [1412.4673](#).
- [3] DUNE collaboration, R. Acciarri et al., *Long-Baseline Neutrino Facility (LBNF) and Deep Underground Neutrino Experiment (DUNE)*, [1512.06148](#).
- [4] JUNO collaboration, F. An et al., *Neutrino Physics with JUNO*, *J. Phys.* **G43** (2016) 030401, [[1507.05613](#)].
- [5] C. D. Froggatt and H. B. Nielsen, *Hierarchy of Quark Masses, Cabibbo Angles and CP Violation*, *Nucl. Phys.* **B147** (1979) 277–298.
- [6] J. Berger and Y. Grossman, *Model of leptons from $SO(3) \rightarrow A(4)$* , *JHEP* **02** (2010) 071, [[0910.4392](#)].
- [7] S. F. King and Y.-L. Zhou, *Spontaneous breaking of $SO(3)$ to finite family symmetries with supersymmetry - an A_4 model*, [1809.10292](#).
- [8] A. S. Joshipura, K. M. Patel and S. K. Vempati, *Type I seesaw mechanism for quasi degenerate neutrinos*, *Phys. Lett.* **B690** (2010) 289–295, [[0911.5618](#)].
- [9] R. Alonso, M. B. Gavela, G. Isidori and L. Maiani, *Neutrino Mixing and Masses from a Minimum Principle*, *JHEP* **11** (2013) 187, [[1306.5927](#)].
- [10] W. Grimus, A. S. Joshipura, L. Lavoura and M. Tanimoto, *Symmetry realization of texture zeros*, *Eur. Phys. J.* **C36** (2004) 227–232, [[hep-ph/0405016](#)].
- [11] Y.-L. Zhou, *Neutrino masses and flavor mixing in a generalized inverse seesaw model with a universal two-zero texture*, *Phys. Rev.* **D86** (2012) 093011, [[1205.2303](#)].
- [12] E. Ma and G. Rajasekaran, *Softly broken $A(4)$ symmetry for nearly degenerate neutrino masses*, *Phys. Rev.* **D64** (2001) 113012, [[hep-ph/0106291](#)].
- [13] G. Altarelli and F. Feruglio, *Tri-bimaximal neutrino mixing from discrete symmetry in extra dimensions*, *Nucl. Phys.* **B720** (2005) 64–88, [[hep-ph/0504165](#)].
- [14] G. Altarelli and F. Feruglio, *Tri-bimaximal neutrino mixing, $A(4)$ and the modular symmetry*, *Nucl. Phys.* **B741** (2006) 215–235, [[hep-ph/0512103](#)].
- [15] P. Ballett, S. Pascoli and J. Turner, *Mixing angle and phase correlations from A_5 with generalized CP and their prospects for discovery*, *Phys. Rev.* **D92** (2015) 093008, [[1503.07543](#)].
- [16] C.-C. Li and G.-J. Ding, *Lepton Mixing in A_5 Family Symmetry and Generalized CP*, *JHEP* **05** (2015) 100, [[1503.03711](#)].
- [17] A. Di Iura, C. Hagedorn and D. Meloni, *Lepton mixing from the interplay of the alternating group A_5 and CP*, *JHEP* **08** (2015) 037, [[1503.04140](#)].
- [18] R. N. Mohapatra, M. K. Parida and G. Rajasekaran, *High scale mixing unification and large neutrino mixing angles*, *Phys. Rev.* **D69** (2004) 053007, [[hep-ph/0301234](#)].
- [19] C. S. Lam, *Determining Horizontal Symmetry from Neutrino Mixing*, *Phys. Rev. Lett.* **101** (2008) 121602, [[0804.2622](#)].
- [20] I. de Medeiros Varzielas, S. F. King and G. G. Ross, *Tri-bimaximal neutrino mixing from discrete subgroups of $SU(3)$ and $SO(3)$ family symmetry*, *Phys. Lett.* **B644** (2007) 153–157, [[hep-ph/0512313](#)].

- [21] I. de Medeiros Varzielas, S. F. King and G. G. Ross, *Neutrino tri-bi-maximal mixing from a non-Abelian discrete family symmetry*, *Phys. Lett.* **B648** (2007) 201–206, [[hep-ph/0607045](#)].
- [22] G.-J. Ding and Y.-L. Zhou, *Predicting lepton flavor mixing from $\Delta(48)$ and generalized CP symmetries*, *Chin. Phys.* **C39** (2015) 021001, [[1312.5222](#)].
- [23] G.-J. Ding and Y.-L. Zhou, *Lepton mixing parameters from $\Delta(48)$ family symmetry and generalised CP*, *JHEP* **06** (2014) 023, [[1404.0592](#)].
- [24] G. Altarelli and F. Feruglio, *Discrete Flavor Symmetries and Models of Neutrino Mixing*, *Rev. Mod. Phys.* **82** (2010) 2701–2729, [[1002.0211](#)].
- [25] S. F. King and C. Luhn, *Neutrino Mass and Mixing with Discrete Symmetry*, *Rept. Prog. Phys.* **76** (2013) 056201, [[1301.1340](#)].
- [26] S. F. King, A. Merle, S. Morisi, Y. Shimizu and M. Tanimoto, *Neutrino Mass and Mixing: from Theory to Experiment*, *New J. Phys.* **16** (2014) 045018, [[1402.4271](#)].
- [27] P. F. Harrison, D. H. Perkins and W. G. Scott, *Tri-bimaximal mixing and the neutrino oscillation data*, *Phys. Lett.* **B530** (2002) 167, [[hep-ph/0202074](#)].
- [28] Z.-z. Xing, *Nearly tri bimaximal neutrino mixing and CP violation*, *Phys. Lett.* **B533** (2002) 85–93, [[hep-ph/0204049](#)].
- [29] P. F. Harrison and W. G. Scott, *Symmetries and generalizations of tri - bimaximal neutrino mixing*, *Phys. Lett.* **B535** (2002) 163–169, [[hep-ph/0203209](#)].
- [30] X. G. He and A. Zee, *Some simple mixing and mass matrices for neutrinos*, *Phys. Lett.* **B560** (2003) 87–90, [[hep-ph/0301092](#)].
- [31] A. Datta, F.-S. Ling and P. Ramond, *Correlated hierarchy, Dirac masses and large mixing angles*, *Nucl. Phys.* **B671** (2003) 383–400, [[hep-ph/0306002](#)].
- [32] F. Feruglio and A. Paris, *The Golden Ratio Prediction for the Solar Angle from a Natural Model with A_5 Flavour Symmetry*, *JHEP* **03** (2011) 101, [[1101.0393](#)].
- [33] L. L. Everett and A. J. Stuart, *Icosahedral ($A(5)$) Family Symmetry and the Golden Ratio Prediction for Solar Neutrino Mixing*, *Phys. Rev.* **D79** (2009) 085005, [[0812.1057](#)].
- [34] Y. Kajiyama, M. Raidal and A. Strumia, *The Golden ratio prediction for the solar neutrino mixing*, *Phys. Rev.* **D76** (2007) 117301, [[0705.4559](#)].
- [35] M. Fukugita, M. Tanimoto and T. Yanagida, *Atmospheric neutrino oscillation and a phenomenological lepton mass matrix*, *Phys. Rev.* **D57** (1998) 4429–4432, [[hep-ph/9709388](#)].
- [36] V. D. Barger, S. Pakvasa, T. J. Weiler and K. Whisnant, *Bimaximal mixing of three neutrinos*, *Phys. Lett.* **B437** (1998) 107–116, [[hep-ph/9806387](#)].
- [37] S. Davidson and S. F. King, *Bimaximal neutrino mixing in the MSSM with a single right-handed neutrino*, *Phys. Lett.* **B445** (1998) 191–198, [[hep-ph/9808296](#)].
- [38] G. Altarelli, F. Feruglio and L. Merlo, *Revisiting Bimaximal Neutrino Mixing in a Model with $S(4)$ Discrete Symmetry*, *JHEP* **05** (2009) 020, [[0903.1940](#)].
- [39] D. Meloni, *Bimaximal mixing and large θ_{13} in a SUSY $SU(5)$ model based on S_4* , *JHEP* **10** (2011) 010, [[1107.0221](#)].
- [40] DAYA BAY collaboration, F. P. An et al., *Observation of electron-antineutrino disappearance at Daya Bay*, *Phys. Rev. Lett.* **108** (2012) 171803, [[1203.1669](#)].

- [41] DAYA BAY collaboration, F. P. An et al., *Improved Measurement of Electron Antineutrino Disappearance at Daya Bay*, *Chin. Phys.* **C37** (2013) 011001, [[1210.6327](#)].
- [42] RENO collaboration, J. K. Ahn et al., *Observation of Reactor Electron Antineutrino Disappearance in the RENO Experiment*, *Phys. Rev. Lett.* **108** (2012) 191802, [[1204.0626](#)].
- [43] DOUBLE CHOOZ collaboration, F. Ardellier et al., *Double Chooz: A Search for the neutrino mixing angle θ_{13}* , [hep-ex/0606025](#).
- [44] F. Bazzocchi and S. Morisi, *$S(4)$ as a natural flavor symmetry for lepton mixing*, *Phys. Rev.* **D80** (2009) 096005, [[0811.0345](#)].
- [45] F. Bazzocchi, L. Merlo and S. Morisi, *Fermion Masses and Mixings in a $S(4)$ -based Model*, *Nucl. Phys.* **B816** (2009) 204–226, [[0901.2086](#)].
- [46] F. Bazzocchi, L. Merlo and S. Morisi, *Phenomenological Consequences of See-Saw in $S(4)$ Based Models*, *Phys. Rev.* **D80** (2009) 053003, [[0902.2849](#)].
- [47] R. Krishnan, P. F. Harrison and W. G. Scott, *Simplest Neutrino Mixing from S_4 Symmetry*, *JHEP* **04** (2013) 087, [[1211.2000](#)].
- [48] R. de Adelhart Toorop, F. Bazzocchi and L. Merlo, *The Interplay Between GUT and Flavour Symmetries in a Pati-Salam $\times S_4$ Model*, *JHEP* **08** (2010) 001, [[1003.4502](#)].
- [49] C. Hagedorn, S. F. King and C. Luhn, *A SUSY GUT of Flavour with $S_4 \times SU(5)$ to NLO*, *JHEP* **06** (2010) 048, [[1003.4249](#)].
- [50] Z.-h. Zhao, *Understanding for flavor physics in the lepton sector*, *Phys. Rev.* **D86** (2012) 096010, [[1207.2545](#)].
- [51] J. Gehrlein, J. P. Oppermann, D. Schafer and M. Spinrath, *An $SU(5) \times A_5$ golden ratio flavour model*, *Nucl. Phys.* **B890** (2014) 539–568, [[1410.2057](#)].
- [52] J. Gehrlein, S. T. Petcov, M. Spinrath and X. Zhang, *Leptogenesis in an $SU(5) \times A_5$ Golden Ratio Flavour Model: Addendum*, *Nucl. Phys.* **B899** (2015) 617–630, [[1508.07930](#)].
- [53] G.-J. Ding, *TFH Mixing Patterns, Large θ_{13} and $\Delta(96)$ Flavor Symmetry*, *Nucl. Phys.* **B862** (2012) 1–42, [[1201.3279](#)].
- [54] S. Pascoli and Y.-L. Zhou, *The role of flavon cross couplings in leptonic flavour mixing*, *JHEP* **06** (2016) 073, [[1604.00925](#)].
- [55] K. Tsumura and L. Velasco-Sevilla, *Phenomenology of flavon fields at the LHC*, *Phys. Rev.* **D81** (2010) 036012, [[0911.2149](#)].
- [56] E. L. Berger, S. B. Giddings, H. Wang and H. Zhang, *Higgs-flavon mixing and LHC phenomenology in a simplified model of broken flavor symmetry*, *Phys. Rev.* **D90** (2014) 076004, [[1406.6054](#)].
- [57] M. A. Arroyo Urena, J. L. Diaz-Cruz, G. Tavares Velasco, A. Bolanos and H. T. G., *Searching for lepton flavor violating flavon decays at hadron colliders*, *Phys. Rev.* **D98** (2018) 015008, [[1801.00839](#)].
- [58] M. Bauer, T. Schell and T. Plehn, *Hunting the Flavon*, *Phys. Rev.* **D94** (2016) 056003, [[1603.06950](#)].
- [59] K. Huitu, V. Keus, N. Koivunen and O. Lebedev, *Higgs-flavon mixing and $h \rightarrow \mu\tau$* , *JHEP* **05** (2016) 026, [[1603.06614](#)].
- [60] E. Ma, *Quark and Lepton Flavor Triality*, *Phys. Rev.* **D82** (2010) 037301, [[1006.3524](#)].

- [61] T. Kobayashi, Y. Omura, F. Takayama and D. Yasuhara, *Study of lepton flavor violation in flavor symmetric models for lepton sector*, *JHEP* **10** (2015) 042, [[1505.07636](#)].
- [62] S. Pascoli and Y.-L. Zhou, *Flavon-induced connections between lepton flavour mixing and charged lepton flavour violation processes*, *JHEP* **10** (2016) 145, [[1607.05599](#)].
- [63] Y. Muramatsu, T. Nomura and Y. Shimizu, *Mass limit for light flavon with residual Z_3 symmetry*, *JHEP* **03** (2016) 192, [[1601.04788](#)].
- [64] J. Heeck, M. Holthausen, W. Rodejohann and Y. Shimizu, *Higgs in Abelian and non-Abelian flavor symmetry models*, *Nucl. Phys.* **B896** (2015) 281–310, [[1412.3671](#)].
- [65] Y. Muramatsu, T. Nomura, Y. Shimizu and H. Yokoya, *Light flavon signals at electron - photon colliders*, *Phys. Rev.* **D97** (2018) 015003, [[1707.06542](#)].
- [66] I. Esteban, M. C. Gonzalez-Garcia, M. Maltoni, I. Martinez-Soler and T. Schwetz, *Updated fit to three neutrino mixing: exploring the accelerator-reactor complementarity*, *JHEP* **01** (2017) 087, [[1611.01514](#)].
- [67] T. Wang and Y.-L. Zhou, *Neutrino non-standard interactions as a portal to test flavour symmetries*, [1801.05656](#).
- [68] C. Englert, J. Jaeckel, V. V. Khoze and M. Spannowsky, *Emergence of the Electroweak Scale through the Higgs Portal*, *JHEP* **04** (2013) 060, [[1301.4224](#)].
- [69] MUON G-2 collaboration, G. W. Bennett et al., *Final Report of the Muon E821 Anomalous Magnetic Moment Measurement at BNL*, *Phys. Rev.* **D73** (2006) 072003, [[hep-ex/0602035](#)].
- [70] T. Blum, A. Denig, I. Logashenko, E. de Rafael, B. Lee Roberts, T. Teubner et al., *The Muon ($g-2$) Theory Value: Present and Future*, [1311.2198](#).
- [71] MUON G-2 collaboration, J. Grange et al., *Muon ($g-2$) Technical Design Report*, [1501.06858](#).
- [72] F. S. Queiroz and W. Shepherd, *New Physics Contributions to the Muon Anomalous Magnetic Moment: A Numerical Code*, *Phys. Rev.* **D89** (2014) 095024, [[1403.2309](#)].
- [73] V. Keus, N. Koivunen and K. Tuominen, *Singlet scalar and 2HDM extensions of the Standard Model: CP-violation and constraints from $(g-2)_\mu$ and e EDM*, [1712.09613](#).
- [74] M. Lindner, M. Platscher and F. S. Queiroz, *A Call for New Physics : The Muon Anomalous Magnetic Moment and Lepton Flavor Violation*, *Phys. Rept.* **731** (2018) 1–82, [[1610.06587](#)].
- [75] BABAR collaboration, B. Aubert et al., *Searches for Lepton Flavor Violation in the Decays $\tau_{+-} \rightarrow e_{+-} \gamma$ and $\tau_{+-} \rightarrow \mu_{+-} \gamma$* , *Phys. Rev. Lett.* **104** (2010) 021802, [[0908.2381](#)].
- [76] BELLE collaboration, K. Hayasaka et al., *New Search for $\tau \rightarrow \mu \gamma$ and $\tau \rightarrow e \gamma$ Decays at Belle*, *Phys. Lett.* **B666** (2008) 16–22, [[0705.0650](#)].
- [77] K. Hayasaka et al., *Search for Lepton Flavor Violating Tau Decays into Three Leptons with 719 Million Produced $\tau^+\tau^-$ Pairs*, *Phys. Lett.* **B687** (2010) 139–143, [[1001.3221](#)].
- [78] SINDRUM collaboration, U. Bellgardt et al., *Search for the Decay $\mu^+ \rightarrow e^+ e^+ e^-$* , *Nucl. Phys.* **B299** (1988) 1–6.
- [79] MEG collaboration, A. M. Baldini et al., *Search for the lepton flavour violating decay $\mu^+ \rightarrow e^+ \gamma$ with the full dataset of the MEG experiment*, *Eur. Phys. J.* **C76** (2016) 434, [[1605.05081](#)].

- [80] MEG II collaboration, S. Ogawa, *Upgrade of liquid xenon calorimeter in MEG experiment with VUV sensitive MPPCs*, *PoS FPCP2015* (2015) 063.
- [81] Mu2E collaboration, L. Bartoszek et al., *Mu2e Technical Design Report*, [1501.05241](#).
- [82] COMET collaboration, Y. Kuno, *A search for muon-to-electron conversion at J-PARC: The COMET experiment*, *PTEP* **2013** (2013) 022C01.
- [83] F. Feruglio, C. Hagedorn, Y. Lin and L. Merlo, *Lepton Flavour Violation in Models with $A(4)$ Flavour Symmetry*, *Nucl. Phys.* **B809** (2009) 218–243, [[0807.3160](#)].
- [84] F. Feruglio, C. Hagedorn, Y. Lin and L. Merlo, *Lepton Flavour Violation in a Supersymmetric Model with $A(4)$ Flavour Symmetry*, *Nucl. Phys.* **B832** (2010) 251–288, [[0911.3874](#)].
- [85] A. Berlin, S. Gori, T. Lin and L.-T. Wang, *Pseudoscalar Portal Dark Matter*, *Phys. Rev.* **D92** (2015) 015005, [[1502.06000](#)].
- [86] C. Kouvaris, I. M. Shoemaker and K. Tuominen, *Self-Interacting Dark Matter through the Higgs Portal*, *Phys. Rev.* **D91** (2015) 043519, [[1411.3730](#)].
- [87] K. Ghorbani, *Fermionic dark matter with pseudo-scalar Yukawa interaction*, *JCAP* **1501** (2015) 015, [[1408.4929](#)].
- [88] T. Robens and T. Stefaniak, *Status of the Higgs Singlet Extension of the Standard Model after LHC Run 1*, *Eur. Phys. J.* **C75** (2015) 104, [[1501.02234](#)].
- [89] G. M. Pruna and T. Robens, *Higgs singlet extension parameter space in the light of the LHC discovery*, *Phys. Rev.* **D88** (2013) 115012, [[1303.1150](#)].
- [90] S. I. Godunov, A. N. Rozanov, M. I. Vysotsky and E. V. Zhemchugov, *Extending the Higgs sector: an extra singlet*, *Eur. Phys. J.* **C76** (2016) 1, [[1503.01618](#)].
- [91] A. Falkowski, C. Gross and O. Lebedev, *A second Higgs from the Higgs portal*, *JHEP* **05** (2015) 057, [[1502.01361](#)].
- [92] G. Dupuis, *Collider Constraints and Prospects of a Scalar Singlet Extension to Higgs Portal Dark Matter*, *JHEP* **07** (2016) 008, [[1604.04552](#)].
- [93] CMS collaboration, V. Khachatryan et al., *Constraints on the Higgs boson width from off-shell production and decay to Z-boson pairs*, *Phys. Lett.* **B736** (2014) 64–85, [[1405.3455](#)].
- [94] A. Alloul, N. D. Christensen, C. Degrande, C. Duhr and B. Fuks, *FeynRules 2.0 - A complete toolbox for tree-level phenomenology*, *Comput. Phys. Commun.* **185** (2014) 2250–2300, [[1310.1921](#)].
- [95] S. Höche, S. Kuttimalai, S. Schumann and F. Siegert, *Beyond Standard Model calculations with Sherpa*, *Eur. Phys. J.* **C75** (2015) 135, [[1412.6478](#)].
- [96] T. Gleisberg, S. Hoeche, F. Krauss, M. Schonherr, S. Schumann, F. Siegert et al., *Event generation with SHERPA 1.1*, *JHEP* **02** (2009) 007, [[0811.4622](#)].
- [97] A. Buckley, J. Butterworth, L. Lonnblad, D. Grellscheid, H. Hoeth, J. Monk et al., *Rivet user manual*, *Comput. Phys. Commun.* **184** (2013) 2803–2819, [[1003.0694](#)].
- [98] ATLAS collaboration, G. Aad et al., *Search for new phenomena in events with three or more charged leptons in pp collisions at $\sqrt{s} = 8$ TeV with the ATLAS detector*, *JHEP* **08** (2015) 138, [[1411.2921](#)].

- [99] ATLAS collaboration, G. Aad et al., *Search for direct production of charginos and neutralinos in events with three leptons and missing transverse momentum in $\sqrt{s} = 8\text{TeV}$ pp collisions with the ATLAS detector*, *JHEP* **04** (2014) 169, [[1402.7029](#)].
- [100] ATLAS collaboration, G. Aad et al., *Search for supersymmetry at $\sqrt{s}=8\text{ TeV}$ in final states with jets and two same-sign leptons or three leptons with the ATLAS detector*, *JHEP* **06** (2014) 035, [[1404.2500](#)].
- [101] ATLAS collaboration, G. Aad et al., *Search for supersymmetry in events with four or more leptons in $\sqrt{s} = 8\text{ TeV}$ pp collisions with the ATLAS detector*, *Phys. Rev.* **D90** (2014) 052001, [[1405.5086](#)].
- [102] ATLAS collaboration, G. Aad et al., *Search for new phenomena in events with three charged leptons at $\sqrt{s} = 7\text{ TeV}$ with the ATLAS detector*, *Phys. Rev.* **D87** (2013) 052002, [[1211.6312](#)].
- [103] CMS collaboration, S. Chatrchyan et al., *Search for anomalous production of multilepton events in pp collisions at $\sqrt{s} = 7\text{ TeV}$* , *JHEP* **06** (2012) 169, [[1204.5341](#)].
- [104] CMS collaboration, S. Chatrchyan et al., *Search for anomalous production of events with three or more leptons in pp collisions at $\sqrt{s} = 8\text{ TeV}$* , *Phys. Rev.* **D90** (2014) 032006, [[1404.5801](#)].
- [105] C. Degrande, *Automatic evaluation of UV and R2 terms for beyond the Standard Model Lagrangians: a proof-of-principle*, *Comput. Phys. Commun.* **197** (2015) 239–262, [[1406.3030](#)].
- [106] LHC HIGGS CROSS SECTION WORKING GROUP collaboration, D. de Florian et al., *Handbook of LHC Higgs Cross Sections: 4. Deciphering the Nature of the Higgs Sector*, [[1610.07922](#)].
- [107] R. V. Harlander and W. B. Kilgore, *Next-to-next-to-leading order Higgs production at hadron colliders*, *Phys. Rev. Lett.* **88** (2002) 201801, [[hep-ph/0201206](#)].
- [108] C. Anastasiou and K. Melnikov, *Higgs boson production at hadron colliders in NNLO QCD*, *Nucl. Phys.* **B646** (2002) 220–256, [[hep-ph/0207004](#)].
- [109] V. Ravindran, J. Smith and W. L. van Neerven, *NNLO corrections to the total cross-section for Higgs boson production in hadron hadron collisions*, *Nucl. Phys.* **B665** (2003) 325–366, [[hep-ph/0302135](#)].
- [110] H. M. Georgi, S. L. Glashow, M. E. Machacek and D. V. Nanopoulos, *Higgs Bosons from Two Gluon Annihilation in Proton Proton Collisions*, *Phys. Rev. Lett.* **40** (1978) 692.
- [111] T. Gleisberg and S. Hoeche, *Comix, a new matrix element generator*, *JHEP* **12** (2008) 039, [[0808.3674](#)].
- [112] ATLAS collaboration, *Search for new phenomena in events with three or more charged leptons in pp collisions at $\sqrt{s} = 8\text{ TeV}$ with the ATLAS detector*, 2015. [10.17182/hepdata.66248](#).
- [113] G. Cowan, K. Cranmer, E. Gross and O. Vitells, *Asymptotic formulae for likelihood-based tests of new physics*, *Eur. Phys. J.* **C71** (2011) 1554, [[1007.1727](#)].
- [114] ROOT COLLABORATION collaboration, K. Cranmer, G. Lewis, L. Moneta, A. Shibata and W. Verkerke, *HistFactory: A tool for creating statistical models for use with RooFit and RooStats*, Tech. Rep. CERN-OPEN-2012-016, New York U., New York, Jan, 2012.

- [115] L. Heinrich, M. Feickert and K. Cranmer, *diana-hep/pyhf v0.0.8*, Feb., 2018.
10.5281/zenodo.1172961.